*Major subject area:* Biochemistry and Chemical Biology

# Fine interaction profiling of VemP and mechanisms responsible for its translocation-coupled arrest-cancelation

Ryoji Miyazaki[1], Yoshinori Akiyama[1], Hiroyuki Mori[1,*]

[1]Institute for Frontier Life and Medical Sciences, Kyoto University, Kyoto 606-8507, Japan

*Correspondence: hiromori@infront.kyoto-u.ac.jp (H.M.)

## Abstract

Bacterial cells utilize monitoring substrates, which undergo force-sensitive translation elongation arrest, to feedback-regulate a Sec-related gene. *Vibrio alginolyticus* VemP controls the expression of SecD/F that stimulates a late step of translocation by undergoing export-regulated elongation arrest. Here, we attempted at delineating the pathway of the VemP nascent-chain interaction with Sec-related factors, and identified the signal recognition particle (SRP) and PpiD (a membrane-anchored periplasmic chaperone) in addition to other translocon components and a ribosomal protein as interacting partners. Our results showed that SRP is required for the membrane-targeting of VemP, whereas PpiD acts cooperatively with SecD/F in the VemP arrest-cancelation. We also identified the conserved Arg-85 residue in VemP as an essential element for the regulated arrest-cancelation of VemP. We propose a scheme of the arrest-cancelation processes of VemP, which likely monitors late steps in the protein translocation pathway.

## Introduction

In bacteria, the evolutionarily conserved Sec translocon and SecA play essential roles in protein translocation across and integration into the membrane (Rapoport et al., 2017). The translocon consists of three membrane-integrated proteins, SecY, SecE and SecG (Mori and Ito, 2001). SecY forms a channel-like path for substrate secretory proteins (Van den Berg et al., 2004) and is stabilized by SecE (Taura et al., 1993). SecG peripherally binds to SecY (Tanaka et al., 2015) and stimulates the SecA-dependent protein translocation (Nishiyama et al., 1994). SecA, an essential ATPase (Lill et al., 1989), binds to cytoplasmic protrusions in SecY (Mori and Ito, 2006a; Zimmer et al., 2008) and pushes a polypeptide into the translocon (Economou and Wickner, 1994; Erlandson et al., 2008). Secretory proteins are generally synthesized as a precursor with an N-terminal signal sequence recognized by the translocation machinery, including the translocon and SecA, and is cleaved off during translocation. Although bacterial protein secretion to the periplasmic space is thought to occur post-translationally in many cases, some secretory proteins use the signal recognition particle (SRP) pathway, which targets the nascent precursor protein to the translocon (Huber et al., 2005; Shimohata et al., 2005). Notably, even in the latter cases, translocation requires the SecA motor function (Shimohata et al., 2005). The Sec translocon is also utilized for protein integration into the membrane. Membrane proteins typically have no cleavable signal sequence, but their transmembrane (TM) regions act as a signal for integration. SRP binds to the signal sequence equivalent (a TM segment) of a membrane protein and deliverers a ribosome-nascent protein complex (RNC) to the translocon (Steinberg et al., 2018). The RNC binds to the same SecY region as SecA (Frauenfeld et al., 2011; Kuhn et al., 2011). Bacteria also have the SecD/F complex that stimulates protein secretion *in vivo* (Pogliano and Beckwith, 1994) and facilitates the release of a polypeptide from the Sec translocon during a late step in translocation (Matsuyama et al., 1993). Structural and functional analyses have shown that SecD/F is a $H^+$-driven motor, in which its periplasmic domain (P1 head) binds a translocon-engaged substrate (Furukawa et al., 2017) and undergoes a conformational change coupled with the $H^+$ flow (Tsukazaki et al., 2011). The repetitive movements of the P1 head would allow a forward movement of a translocating chain until its release to the periplasm.

Protein translocation and membrane insertion are essential biological processes in all living organisms, and it is reasonable that factors required for the localization are tuned according to cellular demands. Bacteria have acquired unique regulatory mechanisms by which either the expression of one of duplicated translocation/integration factors is specifically induced (V.SecD2/F*2* in *Vibrio alginolyticus* (Ishii et al., 2015) (See the next section) and YidC2 (a membrane chaperone) in *Bacillus subtilis* (Rubio et al., 2005)) or a unique factor is up-regulated (SecA in *Escherichia coli*) (Oliver and Beckwith, 1982) in response to a decline in the relevant transport activity of the cell. To monitor the cellular protein translocation activities and regulate the expression of the relevant factors in real-time, these bacteria utilize a special class of nascent polypeptides, called monitoring substrates (Ito et al., 2018), a class of regulatory nascent polypeptide (Tenson and Ehrenberg, 2002), which undergoes translation elongation arrest. Currently, three proteins are known; *V. alginolyticus* VemP (Ishii et al., 2015), *B. subtilis* MifM (Chiba et al., 2009) and *E. coli* SecM (Nakatogawa and Ito, 2001). Translation of these proteins is arrested by the specific interaction of their intrinsic amino acid sequences, called arrest sequences or arrest motifs, with the components of the ribosome. Remarkably, the arrest motifs of different monitoring substrates are diverse, with no apparent sequence similarities.

A marine bacterium, *V. alginolyticus,* possesses two sets of the *secD/F* genes, designated *V.secD1/F1* and *V.secD2/F2,* whose products utilize $Na^+$- and presumably $H^+$-motive forces, respectively. The bacterium adapts quickly to a salinity change by replacing these SecD/F paralogues (Ishii et al., 2015). While *V.secD1/F1* is expressed constitutively, the expression of *V.secD2/F2* is tightly repressed under $Na^+$-rich growth conditions, but induced under low $Na^+$ growth conditions. The *vemP* gene located upstream of *V.secD2/F2* on the same operon plays an essential role in the regulated expression of *V.secD2/F2*. VemP, a substrate of the Sec machinery, monitors the machinery's activity via its own translocation. It undergoes stable translation-arrest before the canonical termination step under a protein translocation-deficient condition. In this scenario, the stalled ribosome on a *vemP-V.secD2/F2* mRNA destabilizes a stem-loop structure in the *vemP-V.secD2* intergenic region, leading to the exposure of an otherwise masked ribosome binding site for the *V.secD2* gene. Thus, the elongation arrest

allows entry of ribosomes to that site and consequent synthesis of V.SecD2/F2. Importantly, the VemP translation-arrest occurs even under a protein translocation competent condition, but it is rapidly canceled presumably by a translocation-coupled pulling force that drives translocation of VemP.

Our previous *in vivo* studies showed that the majority of VemP has its signal sequence processed even in the arrested state. This strongly suggests that the arrest-cancelation of VemP occurs after its translocation has proceeded beyond the signal sequence processing event on the Sec translocon (Mori et al., 2018). Although this feature of VemP seems suitable for monitoring the SecD/F function, molecular mechanisms of how this is accomplished remain to be elucidated. To understand the detailed mechanism of the VemP-arrest-mediated regulation of the *V.secD2/F2* expression, it is crucial to know the dynamic interactions of VemP with other participating proteins during the arrest and its translocation-coupled cancelation processes.

Site-directed *in vivo* photo-crosslinking is a well-designed technique for analysis of inter- or intra-molecular interactions of proteins in living cells (Chin and Schultz, 2002), wherein a pair of a mutated tRNA and an engineered tyrosyl-tRNA synthetase allows for *in vivo* incorporation of a photo-reactive amino acid analog, *p*-benzoyl-L-phenylalanine (*p*BPA), into any selected positions of a target protein by *amber* suppression (Chin et al., 2002). Upon UV irradiation, *p*BPA in the target protein generates a covalent crosslinking with nearby molecules. Identification of crosslinked partners provides detailed information about interactions with them at an amino acid residue level resolution, proving useful for many studies (Miyazaki et al., 2020). To extend this technique to acquire temporal resolution, we recently developed the PiXie (pulse-chase and *in vivo* photo-crosslinking experiment) method. This new approach entails the use of an ultra-powerful UV irradiator that shortens the UV-irradiation time so that we can combine photo-crosslinking and pulse-chase approaches. It enables us to trace dynamic *in vivo* folding/assembly processes of newly-synthesized proteins with high temporal (in the sub-minute order) and spatial (the amino acid residue level) resolutions (Miyazaki et al., 2018). In this study, we performed a non-biased, systematic PiXie analysis of VemP and investigated the factors that interact with a VemP-nascent polypeptide during its biosynthesis. As a biproduct of the analysis, we also identified an amino acid residue of

VemP participating in the force-sensing regulation. Based on these analyses, we discuss how VemP integrates its translocation and arrest regulation for the real-time feedback regulation of the late step motor protein, SecD/F.

## Results

### *In vivo* crosslinking reveals interaction of a VemP nascent polypeptide with Ffh and PpiD as well as uL22 and translocon.

VemP is a Sec-monitoring substrate in *V. alginolyticus* that monitors cellular protein secretion activity via its own translation arrest (Ishii et al., 2015). To identify proteins interacting with a VemP nascent polypeptide, we conducted a systematic PiXie analysis by expressing in *E. coli* a series of VemP-3xFLAG-Myc (VemP-$F_3$M) derivative having *p*BPA at various positions. We distinguished three VemP species, arrested polypeptide having unprocessed signal sequence (AP-un), arrested polypeptide whose signal sequence has been proteolytically processed (AP-pro), and the full-length mature protein (FL-m) (Mori et al., 2018) based on their mobilities on SDS-PAGE (Figure 1). The site of the *p*BPA-introduction varied from the position for the Leu-9 to the one for Phe-131. In growing cells, VemP was initially produced as the arrested forms, which were converted to FL-m with a half-life of ~0.5 min (Mori et al., 2018). To follow the interaction profiles in this rapid process, we used the PiXie method (Miyazaki et al., 2018) (See Materials and Methods), which indeed revealed the UV irradiation-dependent generation of higher molecular mass bands (indicated by colored arrow-heads) indicative of the formation of crosslinked products (XLs) (Figure 1-figure supplement 1A, B).

An XL of ~30 kDa, observed for the VemP(W124*p*BPA) variant, was immunoprecipitatable with an anti-uL22 antibody (Figure 1B, *right*). The proximity of Trp-124 to uL22 *in vivo* is consistent with a recent cryo-EM study showing that Trp-124 of arrested VemP is positioned close to the ribosomal protein uL22 (Figure 1B, *left*) (Su et al., 2017). VemP(F81*p*BPA) and VemP(T83*p*BPA) generated XLs of ~25 kDa. We envisioned that the crosslinked partner could either be SecE (~14 kDa) or SecG (~12 kDa), small components of the translocon, because VemP engages in the Sec-dependent translocation (Mori et al., 2018). We reasoned that these XLs contained SecG because they reacted with an anti-SecG antibody (Figure 1C and Figure 1-figure supplement 2A) and disappeared in the Δ*secG* strain (VemP(F81*p*BPA); Figure 1-figure supplement 2A). To investigate possible crosslinking with SecY, the main component of the translocon, we used a host strain having a chromosomal *secY*-

121 *his$_{10}$* gene. We detected the SecYxVemP XLs for the VemP derivatives having *p*BPA in a middle region (Arg-74,
122 Asp-76, Leu-78, Asn-82 and Trp-86) of VemP among materials pulled-down by polyhistidine affinity isolation
123 (Figure 1D and Figure 1-figure supplement 3A). Thus, the middle region of the newly synthesized VemP chain
124 contacts the translocon.

125 For this interaction to occur, VemP might use some targeting mechanism that delivers it to the
126 translocon. SecM, the Sec-monitoring substrate in *E. coli* was suggested to depend on the SRP pathway
127 (Nakatogawa and Ito, 2001), which consists of the 4.5S RNA and the signal sequence-recognition subunit, Ffh.
128 We found that VemP also interacts with SRP through the PiXie analysis using a strain carrying chromosomal *ffh-*
129 *his$_{10}$*. Placement of *p*BPA within the signal sequence (Ala-15 position) allowed for the generation of a VemPxFfh
130 XL that was His-tag affinity isolated (Figure 1E and Figure 1-figure supplement 3B). We suggest that SRP
131 recognizes the signal sequence of VemP.

132 Placement of *p*BPA at the C-terminal vicinity of the signal sequence (residue 30 to 60) led to the
133 generation of XLs with apparent molecular sizes of ~75 to100 kDa (Figure 1-figure supplement 1A, B). As partner
134 candidates, we highlighted YidC (~60 kDa) (Kuhn et al., 2017), SecD (~68 kDa) (Tsukazaki, 2018) and PpiD (~69
135 kDa) (an inner membrane-anchored periplasmic chaperone) (Antonoaea et al., 2008) based on their sizes and their
136 involvement in protein translocation. We addressed the possibility of their involvement using their His-tagged
137 derivatives, and found that a XL was His-tag affinity-isolated when a cell with chromosomal *ppiD-his$_{10}$* was used
138 (Figure 1F), but not with the other *his$_{10}$* constructs (Figure 1-figure supplement 3C, D). Furthermore, the XL was
139 immunoprecipitated with an anti-PpiD antibody and were not generated in a Δ*ppiD* cell (Figure 1-figure
140 supplement 2B). These results indicate that PpiD interacts with the VemP region (Tyr-36 to Ser-60) that follows
141 the periplasmic end of the signal sequence.

142 None of the VemP XLs with uL22, Ffh, SecG, SecY and PpiD described above were
143 immunoprecipitated with the anti-FLAG antibody (Figure 1-figure supplement 4), indicating that the VemP
144 component in these XLs lacks the C-terminal tag and, therefore, are in the elongation-arrested state. It follows then

that each of the partner proteins binds to the nascent VemP'-tRNA tethered to the ribosome. In addition to the above XLs, we observed ~37 kDa XLs with a number of VemP*p*BPA derivatives (Figure 1-figure supplement 1), some of which proved to be immunoprecipitable with the anti-FLAG antibody (Figure 1-figure supplement 4). We interpret that these ~37 kDa XLs represent dimer forms of FL-m generated in the periplasm. Thus, we did not analyze these XLs any further. Figure 1A summarizes the crosslinking features of nascent VemP polypeptide.

**The VemP nascent polypeptide interacts sequentially with uL22/Ffh, the translocon, and PpiD**

To gain insight into the timing and order of the molecular interactions involving VemP, we next examined *in vivo* stability of the XLs during the chase period using appropriate *p*BPA variants. The intensities of the radioactivities associated with the arrested and non-crosslinked VemP decreased during the chase period due to the secretion-coupled arrest cancelation. While XLs intensities also declined during the chase (Figures 2A, B, and Figure 2-figure supplement 1A-C), a careful comparison of the decrease rates showed that the kinetics of the XLs decrease did not always coincide exactly with that of the arrested-VemP. While the decrease rates of the SecG- and SecY-XLs and the arrested VemP were almost the same, the uL22- and Ffh-XLs decreased slightly faster than the arrested VemP (Figures 2B, C and Figure 2-figure supplement 1D). These results suggest that Ffh (SRP) and uL22 interact with the arrested VemP polypeptide before targeting to the translocon, in agreement with their cellular functions and localization. This was verified by examining the effect of $NaN_3$, a SecA inhibitor, on the VemP-crosslinkings. $NaN_3$ treatment of cells causes the stabilization of the AP-un form of VemP in living cells (Mori et al., 2018), showing that it prevents VemP from initiating its translocation into the translocon. We found that the $NaN_3$ treatment increased the VemP crosslinking with uL22 and Ffh, but decreased its crosslinking with SecY, SecG, and PpiD (Figure 2-figure supplement 2A, B). These results suggest that the arrested VemP interacts with SRP and uL22 before the interactions with the translocon and PpiD on the membrane. In contrast to the uL22- and Ffh-XLs, the PpiD-XLs decreased more slowly than SecY- and SecG-XLs or the arrested VemP

(Figure 2B, C). This suggests that VemP is recognized by PpiD after it engages with the translocon, being consistent with the topology of PpiD that has a functional domain in the periplasm.

**Ffh (SRP) functions in the targeting of VemP**

We examined the role of Ffh (SRP) in the membrane translocation and arrest-cancelation of VemP by pulse-chase experiments using an *E. coli* strain, WAM121, in which *ffh* is transcribed from the arabinose promoter (de Gier et al., 1996). The Ffh-depletion upon removal of arabinose from the medium stabilized the AP-un form of VemP (Figure 3A), indicating an impairment of the targeting of the VemP-ribosome complex to the translocon. The prolonged translation-arrest of VemP is expected to induce the expression of the downstream *V.secD2/F2* genes (Ishii et al., 2015). To verify this point, we examined the V.SecD2 expression in WAM121 cells carrying a *vemP-V.secD2/F2* plasmid, and found that the synthesis of V.SecD2 was indeed elevated under the Ffh-depleted conditions (Figure 3B). We also examined the effect of an Ffh-depletion on the V.SecD2 expression in the cognate organism, *V. alginolyticus* (Figure 3C). Under a $Na^+$-rich growth condition, the $Na^+$-driven V.SecD1/F1 in this organism was fully functional, leading to the efficient arrest cancelation of VemP and consequent tight repression of V.SecD2 (Ishii et al., 2015). In the Ffh-depletable strain of *V. alginolyticus* with the arabinose promoter-controlled *ffh*, the V.SecD2 expression was induced in the arabinose-free medium even in the presence of a sufficient level of $Na^+$, consistent with the notion that the Ffh-depletion compromises the targeting of VemP and stabilizes its translation arrest. These results suggest that SRP is crucial for the translocon targeting of VemP, which is a prerequisite for the proper regulation of the V.SecD2/F2 expression in *Vibrio*.

**PpiD and SecD/F cooperate to facilitate the translocation and the arrest cancelation of VemP**

We then carried out functional studies of PpiD, identified in this study as a crosslinking partner of VemP. Pulse-chase analysis showed that VemP was kept in the arrested state much more stably in the Δ*ppiD* cells than in the *ppiD*$^+$ *E. coli* cells (Figure 4A). We note that translocation of a secretory protein MBP (maltose-binding

192 protein) was also retarded by the *ppiD* disruption, albeit less pronouncedly (Figure 4A). The loss of *ppiD* increased
193 the V.SecD2 expression in *E. coli* (Figure 4B) and in *Vibrio* (Figure 4C). These results show that PpiD plays a
194 crucial role in the arrest-cancelation of VemP. The PpiD disruption caused an accumulation of the AP-pro form
195 of VemP in contrast to the Ffh depletion that led to the AP-un accumulation (compare Figures 3A and 4A). These
196 results support the notion that PpiD acts on the periplasmic side after the signal sequence cleavage of the arrested
197 VemP, whereas Ffh acts earlier on the cytosolic side. Our kinetic analysis already showed that PpiD is crosslinked
198 to VemP at a late step of its translocation processes (Figure 2).
199 Next, we addressed how PpiD participates in the arrest cancelation of VemP, whose role is to regulate
200 the expression of SecD/F that facilitates a late step of translocation (Mori et al., 2018). The role of SecD/F itself
201 in the VemP arrest cancelation can be seen from the prolonged VemP arrest in the *secD1* (a mutation causing
202 SecD/F depletion) *E. coli* cells (Figure 4D, vector lanes) and the enhanced arrest cancelation by overproduction
203 of SecD/F (Figure 4D, *left*, vector vs. *secD/F*). As both SecD/F and PpiD are involved in later steps of VemP
204 translocation, they might cooperate in canceling the elongation arrest. Alternatively, they might have redundant
205 functions. The arrested state of VemP was stabilized in the Δ*ppiD* cells (Figure 4D, vector lanes), showing that its
206 function is required for the active translocation and the arrest cancelation of VemP. Whereas the overproduction
207 of PpiD facilitated the arrest cancelation, as expected, SecD/F's overproduction was ineffective in relieving the
208 arrested state due to the *ppiD* defect. Conversely, PpiD overproduction was ineffective in relieving the arrested
209 state due to the *secD1* mutation (Figure 4D). These results rule out the possibility that the roles of SecD/F and
210 PpiD in arrest cancelation are redundant. Instead, both of them are specifically required for the cancelation of
211 VemP arrest, raising the possibility that they interact with each other. We then studied this point by *in vivo* photo-
212 crosslinking. When *p*BPA was incorporated into the position of Asp-359 in the P1 head of SecD, its XLs with
213 PpiD were detected (Figure 4E). Thus, PpiD resides in close proximity to the mobile P1 head of SecD of the
214 VemP-translocating translocon.
215

**Conserved Arg-85 has a role in the regulation of secretion-coupling of the VemP arrest cancelation**

Our systematic *p*BPA scanning incidentally revealed that incorporation of this amino acid analog to some VemP residues compromised the translation arrest of VemP (Figure 1-figure supplement 1A and Figure 5-figure supplement 1A). We selected several residues among them (shown in Figure 5-figure supplement 1B**),** and replaced them individually with Trp (having a bulky, hydrophobic side chain like *p*BPA). The Trp substitutions destabilized the translation arrest in similar ways to the corresponding *p*BPA substitutions. Among them, the R85W mutation had the strongest effect; it decreased the ratio of arrested forms to total VemP to the level comparable with that observed with a previously identified arrest motif mutation, W143A (Mori et al., 2018). Several other replacements of Arg-85 by residues of different properties also impaired apparently the translation arrest of VemP (Figure 5A, B). The R85W mutation abrogated the arrest-mediated up-regulation of *V.secD2* (Figure 5-figure supplement 1C). These results showed that Arg-85 is crucial for the stable translation arrest of VemP *in vivo*.

We conceived two possibilities that account for the observed phenotypes of the Arg-85 mutations. First, this residue belongs to the arrest sequence, although it presumably resides outside of the ribosome in the arrested translation complex. In this case, the Arg-85 mutations simply lead to a loss of arrest proficiency. Secondly, Arg-85 regulates the arrest proficiency by partially antagonizing the secretion-coupled arrest cancelation. In this scenario, the Arg-85 mutation may sensitize the VemP nascent chain to the secretion-generated pulling force and consequently lead to the apparent arrest-defective phenotype *in vivo*. To distinguish these possibilities, we examined the VemP(R85W) mutant protein behaviors under secretion-defective conditions. In the Sec-deficient cells (see Materials and Methods), the arrested form of WT VemP was stabilized (Mori et al., 2018), while that of VemP(W143A) was rapidly converted to the full-length form (Figure 5C). In contrast, the R85W mutant did not exert a negative effect on the arrest in the secretion-impaired cell (Figure 5C). As another means to render VemP indifferent to secretion, we deleted its signal sequence. The R85 mutation did not affect the elongation arrest in the absence of the signal sequence. By sharp contrast, the W143A mutation abolished the arrest even in the absence

240 of the signal sequence (Figure 5-figure supplement 1D). Thus, the mode of involvement of Arg-85 in the
241 elongation arrest is fundamentally different from that of Trp-143.
242 The Arg-85 residue seems to have a regulatory role by which the secretion-sensitivity of the arrested state of VemP
243 is tuned appropriately. Such a mechanism could repress the arrest cancelation of VemP until translocation of VemP
244 proceeds to an appropriate stage, at which PpiD and SecD/F come in to enhance the late stage of translocation.
245

## Discussion

VemP in *Vibrio* controls the SecD/F expression through its force-sensitive translation arrest. Although we previously suggested that the arrest cancelation of VemP is coupled to a late step of translocation (Mori et al., 2018), the details of the responsible force and how this regulatory process occurs remain largely unknown. To understand the molecular mechanisms that lead to the elongation arrest and its cancelation, we performed a systematic PiXie analysis of VemP, which allowed us to identify cellular factors that sequentially interact with the newly-synthesized VemP polypeptide chain. We previously used the PiXie method, which allows precisely time-controlled and residue-specific crosslinking, to analyze the post-translational maturation processes of protein complexes with different cellular localizations in bacteria (Miyazaki et al., 2018). This method should also be useful for studying co-translational events (Kramer et al., 2019; Pechmann et al., 2013) that a nascent polypeptide experiences during translation. In particular, a class of polypeptides that undergoes translation arrest would be suitable targets of the PiXie analysis. The molecular interaction behaviors of such arrest peptides, including bacterial VemP, SecM, MifM and mammalian XBP1u (Chiba et al., 2009; Ishii et al., 2015; Nakatogawa and Ito, 2002; Yanagitani et al., 2011), would be highly relevant for our understanding of these nascent polypeptides in the cell. Thus, in this work, we applied the PiXie method to VemP, which we have identified and characterized previously (Ishii et al., 2015).

We identified Ffh and PpiD as factors directly interacting with the arrested VemP in addition to the ribosomal protein uL22 and the translocon components (Figure 1). Our experiments demonstrated their sequential interactions with VemP (Figure 2); VemP initially interacts with uL22 and the cytosolic Ffh, then with the membrane-embedded translocon, and lastly with PpiD, a periplasmically exposed chaperone. The crosslinking of VemP with Ffh and PpiD should have functional significance rather than representing a result of a non-specific collision of VemP with these proteins, as suggested by our genetic analyses using the Ffh-depletable and the *ppiD* deletion strains. The observation that the distinct regions in VemP interact with uL22, Ffh, the translocon, and PpiD (Figures 1 and 6A, *left*) is consistent with pre-targeting interactions of the arrested VemP with uL22 and Ffh

and a post-targeting interaction with PpiD (Figure 6A, *right*). A cryo-EM study showed that a VemP nascent polypeptide in the ribosomal exit tunnel forms a compacted secondary structure (Su et al., 2017). In this structure, Trp-124 of VemP contacts the uL22 protein. Our PiXie study has shown that this interaction occurs *in vivo*. Interestingly, we found that the crosslinking representing the VemP-uL22 interaction was enhanced markedly when cells were treated with $NaN_3$ that should have compromised an early step of the VemP translocation by inhibiting SecA. Thus, the VemP's interaction with uL22 occurs before its initial insertion into the translocon (Figure 2-figure supplement 2).

We suggest that VemP in the ribosomal tunnel changes its conformation from the compacted state to some other state, perhaps a more extended one, as the translocation process proceeds, because the structural determination had used a nascent chain-ribosome complex without any translocation factors (Su et al., 2017) (Figure 6A, *right*). It is conceivable that a pulling force generated by translocation acts to disrupt the VemP secondary structure and, consequently, the molecular interactions required for the elongation arrest.

We propose the following scheme for the targeting and translocation processes of VemP accompanied by the translation-arrest and its cancelation (Figure 6B). (*i*) In the cytosol, SRP recognizes and binds to the signal sequence of VemP and targets the nascent chain to the translocon. During this co-translational targeting step, the ongoing translation of VemP is subject to elongation arrest. The use of the SRP pathway, in conjunction with the amino acid sequence features of its signal sequence (Yap and Bernstein, 2011) and the early mature part (see below), might ensure the timely release of the translation complex from the translation-arrested state. (*ii*) The signal sequence is then inserted into the lateral gate region while the mature region of VemP is going to span the translocon's polypeptide-conducting channel. This early step of translocation is facilitated by the SecA ATPase and accompanied by the signal sequence cleavage. Therefore, the inhibition of SecA with $NaN_3$ causes accumulation of the AP-un form of VemP. (*iii*) SecD/F and PpiD then interact with VemP and cooperate in canceling the translation arrest of VemP while aiding its further translocation. (*iv*) Finally, the full-length, mature VemP polypeptide is exported to the periplasm.

In the arrest cancelation event, PpiD and SecD/F seem to cooperate either sequentially or in concert, and our crosslinking results revealed that they physically interact with each other (Figure 4E). PpiD was a member of the periplasmic chaperone network (Dartigalongue and Raina, 1998; Matern et al., 2010), which directly interacts with both SecY/E/G and ribosome-tethered polypeptides (Antonoaea et al., 2008; Sachelaru et al., 2014). Whereas an *in vitro* study revealed that PpiD stimulates translocation of substrate proteins (Fürst et al., 2018), the deletion of the *ppiD* gene caused no detectable defect of outer membrane protein biogenesis (Justice et al., 2005). We found that the translocation of MBP was compromised weakly in the Δ*ppiD* strain (Figure 4A). At any rate, the exact role of PpiD in protein export remains obscure. We showed here that PpiD physically contacts SecD as well as the AP-pro form of VemP *in vivo*. Furthermore, our genetic and biochemical analyses indicated that PpiD has a role in the cancelation of the VemP translation arrest (Figure 4). Although our experiments failed to detect a VemP-SecD crosslinking, due possibly to the transient/unstable nature of their interaction, SecD/F also functions in the arrest cancelation of VemP (Figure 4D). We propose that PpiD and SecD/F cooperate to facilitate translocation and arrest-cancelation of VemP.

SecD/F works as a monovalent cation-driven motor that pulls up a translocating polypeptide by undergoing a conformational change of the P1 head (Tsukazaki et al., 2011). Such an action could generate a pulling force that cancels the VemP elongation arrest. By contrast, PpiD itself would not generate a pulling force against the nascent chain because it is an ATP-independent chaperone (Matern et al., 2010). It is conceivable that PpiD captures a VemP polypeptide emerging from the translocon and then hand it over to the P1 head domain, which is known as the substrate-binding site of SecD (Furukawa et al., 2017). Possibly, the direct contact between PpiD and SecD facilitates the substrate transfer from PpiD to SecD. It is also possible that the binding of VemP by PpiD helps to prevent the reverse movement of VemP. Although further studies including identification of contact sites of PpiD with the P1 head of SecD and the detailed *in vitro* study of the late step translocation of VemP and other substrates are needed, it is noteworthy that bacterial species appear to be equipped with a dedicated pulling system acting from the extra cytosolic location for protein secretion and translational control.

We identified Arg-85 as a *cis*-element important for the *in vivo* stability of the translation-arrest of VemP, through its role in the regulation of the translocation coupling of the arrest-cancelation. Arg-85 is highly conserved among the VemP orthologues (Figure 5-figure supplement 2), pointing to its importance in the VemP function. This residue does not contribute to the establishment, *per se*, of the translation-arrested state of VemP, when its secretion is blocked. However, under the export-proficient conditions, Arg-85 somehow represses the premature cancelation of the arrest (Figure 5). Our crosslinking results show that a region encompassing the Arg-74 to Trp-86 interval interacts with the translocon's components in the arrested state of VemP (Figure 6A), indicating that Arg-85 resides in the SecY/E/G-contacting region of the VemP nascent chain (Figure 6A). This spatial arrangement leads us to assume that Arg-85 somehow interacts with the translocon, which stabilizes the elongation-arrested state by antagonizing the translocation force that otherwise (when Arg85 is mutated) could lead to a rapid arrest cancelation. Thus, a force strong enough to overcome the arrest must be applied in the case of wild-type VemP to make it competent for regulation.

It is conceivable that the presence of Arg-85 acts as a potential obstacle for translocation. However, the trans-side motor SecD/F with the aide from PpiD might overcome the obstacle and manage to allow translocation and arrest-cancelation to take place with a physiological efficiency. When Arg-85 is mutated to other amino acid residues, translocation does not meet any obstacle and proceed very rapidly such that we do not see any significant arrest in the Sec-proficient cells. When the signal sequence of VemP is non-functional or the Sec system is inactivated, the elongation arrest occurs normally and continues stably whether or not Arg85 is mutated. Alternatively, the interaction of Arg-85 with the translocon could stabilize the ribosome-translocon interactions preferably over the translocon-SecA interaction, inducing the dropping-out of SecA from the translocon, as the ribosome and SecA share the same binding sites in SecY (Frauenfeld et al., 2011; Zimmer et al., 2008). This situation would lead to the shutoff of the pulling force supply by SecA, making stabilization of the arrested state of VemP until the PpiD-SecD/F system starts pulling the substrate.

In either case, the VemP arrest cancelation may require a pulling force by the PpiD-SecD/F system in addition to the force generated by SecA, which alone is insufficient. From this line of considerations, we propose that translation and translocation of VemP are tuned to monitor the periplasmic motor activity of the bacterial Sec system. Remarkably, monitoring substrates employ different force-generation mechanisms to enable real-time monitoring of local events of polypeptide translocation, which is superimposed with temporal elements of translation. The notion that the conserved Arg-85 residue confers the PpiD-SecD/F dependency of the arrest-release of VemP requires further experimental verification, including *in vitro* recapitulation of arrest cancelation by SecA plus ATP vs PpiD-SecD/F plus proton/sodium-motive forces. A single-molecule analysis to measure the pulling force required for the arrest-release of VemP will also be informative.

Interestingly, SecM also possesses a *cis*-element that is located outside the ribosome in the arrested translation complex and required for the efficient arrest cancelation (Ito et al., 2018; Nakamori et al., 2014). The regulatory target of SecM is SecA (Nakatogawa and Ito, 2001), and its arrest is canceled at an early stage of translocation, before the cleavage of the signal sequence (Mori et al., 2018; Nakatogawa and Ito, 2001). SecM may monitor the SecA-stimulated early translocation event. Our current results, taken together, reveal that different monitoring substrates monitor different sub-steps of translocation, and a cis-element aids the monitoring function by different mechanisms. Our results suggest that pulling forces applied to the ribosome-nascent-chain complexes can be diverse and differentiated to be sensed and processed precisely by regulatory nascent polypeptides, opening up a new dimension of the force-sensing translation arrest.

# Materials and Methods

## Key resources table

| Reagent type or resource | Designation | Source reference | Identifiers | Additional information |
|---|---|---|---|---|
| Strains | *E. coli*<br>*V. alginolyticus* | This study | N/A | Supplementary file 1 |
| Virus | P1 bacteriophage | Laboratory stock | CGSC12133 | |
| Recombinant DNA | Plasmids | This study | N/A | Supplementary file 2 |
| Oligonucleotides | | This study | PCR primers | Supplementary file 3 |
| Antibodies | 1st antibodies | This study | N/A | listed in the below |
| Antibody | Goat Anti-Rabbit IgG (H + L)-HRP Conjugate | Bio-Rad Laboratories | 1706515 | |
| Chemical compound | H-p-Bz-Phe-OH | Bachem | F2800 | |
| Chemical compound | Methionine, L-[$^{35}$S] Translation Grade | American Radiolabeled Chemicals | ARS 01014 | |
| Chemical compound | ANTI-FLAG M2 Affinity Gel | Sigma-Aldrich | A2220 | |
| Chemical compound | nProtein A Sepharose™ 4 Fast Flow | GE Healthcare | 17528004 | |
| Chemical compound | Ni-NTA Agarose | QIAGEN | 30250 | |
| Critical Commercial Assays | ECL™ Western Blotting Detection Reagents | GE Healthcare | RPN2106 | |
| Critical Commercial Assays | ECL™ Prime Western Blotting Detection Reagents | GE Healthcare | RPN2232 | |
| Software, Algorithm | Microsoft Excel | Microsoft | N/A | |
| Software, Algorithm | Bio-imaging Analyzer BAS-1800 | Fujifilm/GE Healthcare | N/A | |
| Software, Algorithm | Image Qaunt LAS 4000 mini | Fujifilm/GE Healthcare | N/A | |
| Software, Algorithm | Multi Gauge | Fujifilm/GE Healthcare | N/A | |

## Bacterial strains, Plasmids and Primers

*Escherichia coli* K12 strains and *Vibrio alginolyticus* VIO5 strains, plasmids and primers used in this study are listed in Supplementary files 1, 2, and 3, respectively. Details of the strain and plasmid construction are described in Construction of Mutant Strains and Plasmid Construction, respectively.

367

368 **Media and Bacterial Cultures**

369 *E. coli* cells were grown in L rich medium (10 g/L bacto-tryptone, 5 g/L bacto-yeast extract, 5 g/L NaCl; pH
370 adjusted to 7.2 with NaOH; (Miller, 1972)) or M9 synthetic medium (without $CaCl_2$; (Miller, 1972)) supplemented
371 with maltose (final 0.2%), glycerol (final 0.4%), all amino acids (except Met and Cys; final concentration of 20
372 µg/mL each). 50 µg/mL ampicillin, 20 µg/mL chloramphenicol, 25 µg/mL kanamycin, 25 µg/mL tetracycline and
373 50 µg/mL spectinomycin were added as appropriate for growing plasmid-bearing cells and selection of
374 transformants and transductants. *V. alginolyticus* cells were grown in VC rich medium (5 g/L bacto-tryptone, 5
375 g/L bacto-yeast extract, 4 g/L $K_2HPO_4$, 30 g/L NaCl, 2 g/L glucose; (Terashima et al., 2010)). For induction with
376 arabinose, we used modified VC medium containing 0.2% arabinose instead of 0.2% glucose. 2.5 µg/mL
377 chloramphenicol was added as appropriate for growing plasmid-bearing cells. Bacterial growth was monitored
378 with Mini photo 518R (660 nm; TAITEC Co., Saitama, Japan).

379

380 **Antibodies**

381 ANTI-FLAG M2 Affinity Gel (anti-FLAG antibody for immunoprecipitation) was purchased from Sigma-Aldrich,
382 Co. LLC (St. Louis, MO). For preparation of an antibody against SecD, two oligopeptides (CYKDSGKKDANG
383 and CYGGKRVLLLSI) were synthesized. They were mixed, conjugated with a carrier protein, keyhole limpet
384 hemocyanin, via the Cys residue attached at their N-terminus and used to raise antibodies in rabbits. Anti-SecD
385 IgGs were affinity-purified and used in the experiments. Anti-uL22, anti-Ffh, and anti-PpiD antibodies were gifts
386 from S. Chiba (Kyoto Sangyo University, Kyoto, Japan), C. A. Gross (University of California at San Francisco,
387 San Francisco, CA) and M. Müller (University of Freiburg, Freiburg, Germany), respectively. Anti-VemP, anti-
388 V.SecD1, and anti-V.SecD2 (Ishii et al., 2015), antibodies as well as anti-SecG (Nishiyama et al., 1993) and anti-
389 MBP (Baba et al., 1990) antibodies were described previously.

390

391 **Construction of Mutant Strains**

392 RM3122 (HM1742, Δ*secG*::*kan*) and RM3124 (HM1742, Δ*ppiD*::*kan*) was constructed by transducing
393 Δ*secG*::*kan* from JW3142 (Baba et al., 2006) and Δ*ppiD*::*kan* from JW0431 (Baba et al., 2006) to HM1742 (Mori
394 and Ito, 2006b). RM2831 (HM1742, *ffh-his*$_{10}$) were constructed by essentially the same procedure as the
395 construction of SPA-tag collection strains (Butland et al., 2005). First, a *his*$_{10}$*-tag*::*kan* fragment having sequences
396 identical to the upstream and downstream regions of the *ffh* termination codon at its 5' and 3' ends, respectively,
397 was PCR-amplified from pRM573 (See the last part of this session) using ffh-his$_{10}$-f and ffh-his$_{10}$-r primers. Then,
398 this fragment was integrated into the *E. coli* DY330 chromosome using the λ-Red recombination system (Yu et
399 al., 2000). After transferring an *ffh-his*$_{10}$*-tag*::*kan* to HM1742 by P1 transduction, the *kan* cassette was removed
400 using pCP20 to yield RM2831. RM2834 (HM1742, *secY-his*$_{10}$) was constructed in a similar way, except that a
401 different pair of the primers, secY-his$_{10}$-f and secY-his$_{10}$-r were used. RM2935 (HM1742, *yidC-his*$_{10}$ kan) and
402 RM3032 (HM1742, *ppiD-his*$_{10}$ kan) were also constructed similarly using the primer pairs, yidC-his$_{10}$-f/yidC-
403 his$_{10}$-r and ppiD-his$_{10}$-f/ppiD-his$_{10}$-r, respectively while the *kan* cassettes of these strains were not removed.
404 *Vibrio* mutant strains RMV2 and RMV7 were constructed using a "suicide vector", pSW7848, carrying the toxin-
405 encoding *ccdB* gene under the arabinose promoter control (Ishii et al., 2015). 150 μL of an overnight culture of *E.*
406 *coli* β3914 cells harboring pRM691 or pRM744 was mixed well with 50 μL of an overnight culture of *V.*
407 *alginolyticus* VIO5 strain. Cells were harvested and resuspended in 100 μL of the VC medium and 2.5 μL of the
408 suspensions was spotted on the VC agar medium containing 300 μM 2,6-diaminopimelic acid (DAP) and incubated
409 at 30°C for 6 h. Then the cells were streaked on a VC plate containing 2.5 μg/mL chloramphenicol but without
410 DAP to select *Vibrio* cells in which a plasmid had been integrated on the chromosome. Subsequently, the
411 chloramphenicol-resistant bacteria were grown on VC-0.2% arabinose agar plates to counter-select the plasmid-
412 integrated *Vibrio* cells. After confirmation of chloramphenicol-sensitivity and arabinose resistance of obtained
413 cells, presence of the introduced mutations was confirmed by colony PCR.
414

**Plasmids Construction**

pTS48 was constructed in the same way as the construction of pTS47 (pHM1021-*vemP-3xflag-myc*; (Mori et al., 2018)). pRM374 (pTV118N-*vemP-3xflag-myc*) was constructed by subcloning a NcoI-HindIII fragment carrying the *vemP-3xflag-myc* prepared from pTS48 into the same sites of pTV118N. pHM1021-*vemP(amb)-3xflag-myc* plasmids and pTV118N-*vemP(amb)-3xflag-myc* plasmids shown in Supplementary file 2 were constructed as follows. An *amber* mutation at the codons corresponding to the amino acid residues, F11, M16, A21, F24, K31, Y36, Q41, S46, N51, F56, E61, S66, S71, D76, F81, W86, R91, D96, V101, N106, V111, D121, Q126, F131 or S136 was introduced into pTS48 by site-directed mutagenesis using a pair of appropriate primers. Then, pTV118N-*vemP-3xflag-myc* plasmids containing the same *amber* mutation was constructed by cloning the NcoI-HindIII fragments that had been prepared from the resultant pHM1021-based plasmids into the same sites of pTV118N. For construction of plasmids carrying an *amber* codon at positions of the other amino acid residues, an *amber* mutation was first introduced into pRM374 by site-directed mutagenesis. For construction of pHM1021-*vemP-3xflag-myc* plasmids containing the same *amber* mutation, the NcoI-HindIII fragments were prepared from the pRM374-based plasmids and sub-cloned into the same sites of pHM1021. Derivatives of pTS48 encoding a VemP-$F_3$M mutant with an amino acid alteration were constructed by site-directed mutagenesis. pRM662 (pBAD24-*vemP(R85W)-V.secD2/F2*) was constructed from pHM810 (pBAD24-*vemP-V.secD2/F2*; (Ishii et al., 2015)) by site-directed mutagenesis. The pHM1021-*vemP-secDF2*$_{VA}$ (pRM663), pHM1021-*vemP(W143A)-V.secD2/F2* (pRM666) and pHM1021-*vemP(R85W)-V.secD2/F2* (pRM667) plasmids were constructed by subcloning the NcoI-SphI fragment carrying the *V.vemP-secD2/F2* genes with or without the respective mutations that had been prepared from pBAD24-*V.vemP-secD2/F2* plasmids (pHM810, pHM846 and pRM662, respectively). pRM520 (pTV118N-*his*$_{10}$*-vemP-3xflag-myc*) was constructed as follows. A *his*$_{10}$*-vemP-3xflag-myc* fragment was PCR-amplified from pTS48 using his$_{10}$-vemP-f and M4C primers, digested with NcoI and HindIII, and cloned into the same sites of pTV118N. pRM557 (pTV118N-*his*$_{10}$*-vemP(ΔSS)-3xflag-myc*) was constructed

by site-directed mutagenesis of pRM520. Derivatives of pRM557 (pRM562 and pRM563) containing a mutation in the *vemP* gene were also constructed by site-directed mutagenesis.

pRM83c was a constitutive expression vector, in which the operator region *lacO1* on the *lac* promoter of pRM83 (Miyazaki et al., 2016) had been converted from AATTGTGAGCGGATAACAATT to AATTATTGTTAGACAATAATT (the mutated residues are underlined) by successive site-directed mutagenesis as follows. First, the operator region *lacO1* of pRM83 was changed from AATTGTGAGCGGATAACAATT to AATT**A**T**TGT**CGGATAACAATT using lacO1-c-f and lacO1-c-r primers (the mutations introduced were shown in bold). The second mutagenesis was done with the resultant plasmid as a template using lacO1-c2-f and lacO1-c2-r primers to introduce two additional mutations (AATTATTGTCGGA**C**AA**T**AATT). Finally, further site-directed mutagenesis (AATTATTGT**TA**GACAATAATT) was conducted using lacO1-c3-f and lacO1-c3-r primers to obtain pRM83c. pRM656 (pRM83c-*his*$_{10}$*-secD/secF*) was constructed as follows. A *his*$_{10}$*-secD/secF* fragment was PCR-amplified from pHM735 (Tsukazaki et al., 2011) using his$_{10}$-secD-f and secF-r primers, digested with HindIII and SalI, and cloned into the same sites of pRM83c. To reduce the expression level of SecD/SecF, the start codon (ATG) for *secD* on the above plasmid was mutated to TTG by site-directed mutagenesis. pRM661 (pRM83c-*ppiD*) was constructed as follows. A *ppiD* fragment was PCR-amplified from a *ppiD-his*$_{10}$ plasmid (laboratory stock) using ppiD-f and ppiD-r primers, digested with HindIII and SalI, and cloned into the same site of pRM83c.

The plasmid used for construction of RMV2 (VIO5, Δ*ppiD*) was constructed as follow. First, a DNA fragment containing a *V.ppiD* gene with an (1 kb) upstream and downstream sequences was amplified from the genome of VIO5 using Va-ppiD-f and Va-ppiD-r primers, and ligated with the BamHI- and SalI-digested pUC118 fragment using In-Fusion HD cloning Kit to generate pRM670. Next, a DNA fragment for the *V.ppiD*-upstream and downstream region with the entire vector sequence was amplified from pRM670 by PCR using del-Va-ppiD-f and del-Va-ppiD-r primers, and self-ligated using In-Fusion HD cloning Kit to produce pRM674. Finally, ~2 kbp DNA fragment containing *V.ppiD*-upstream and -downstream regions was amplified from a pRM674 using

462 pSW-ppiD-f and pSW-ppiD-r primers, and ligated with the NaeI-digested pSW7848 using In-Fusion HD cloning
463 Kit to construct pRM691. The plasmid used for construction of RMV4 (VIO5, $P_{ara}$-*V.ffh*) was constructed as follow.
464 First, a DNA fragment containing an *V.ffh* gene was amplified from the genome of VIO5 using Va-ffh-f and Va-
465 ffh-r primers, and ligated with the NcoI- and SphI-digested pBAD24 fragment using In-Fusion HD cloning Kit to
466 generate pRM737. Next, an *V.ffh*-upstream region that had been amplified from the VIO5 genome using u-ffh-f
467 and u-ffh-r primers and a DNA fragment that had been amplified from the pRM737 using pRM737-f and pRM737-
468 r were ligated using In-Fusion HD cloning Kit to generate pRM740. Finally, ~3.8 kbp DNA fragment was
469 amplified from the pRM740 plasmid using pSW-ffh-f and pSW-ffh-r primers, and ligated with the NaeI-digested
470 pSW7848 using In-Fusion HD cloning Kit to construct pRM744.
471 pRM570 (a plasmid carrying the *spa-tag* and a *kan* cassette *sequences* (*spa-tag*::*kan*)) was constructed
472 as follow. A *spa-tag*::*kan* fragment was amplified from the genome of an *ffh-spa-tag* strain (Butland et al., 2005)
473 using spa-kan-f and spa-kan-r primers, digested with EcoRI and SalI, and cloned into the same sites of pUC118.
474 The stop codon of *spa-tag* was changed from TAG to TAA by site-directed mutagenesis to generate pRM570. To
475 construct pRM573 (pUC118-$his_{10}$-*tag*::*kan*), a $his_{10}$-*tag*::*kan* fragment was amplified from pRM570 using $his_{10}$-
476 kan-f and M4C primers, digested with EcoRI and SalI, and cloned into the same sites of pUC118. To construct
477 pRM741, a *kan cassette* fragment was amplified from pRM570 using kan-Para-f and kan-Para-r primers, and
478 ligated with NsiI-digested pRM740 using In-Fusion HD cloning Kit.
479
480 **Immunoblotting analysis**
481 This method was used in Figures 3A–C, 4C–E and Figure 5-figure supplement 1D. Solubilized total proteins were
482 separated by SDS-PAGE and electro-blotted onto a PVDF membrane (Merck Millipore; Billerica, MA). The
483 membrane was first blocked with 5% skim milk in PBST (Phosphate Buffered Saline with Tween 20), and then
484 incubated with anti-SecD (1/2,000 dilution), anti-V.SecD1 (1/2,000), anti-V.SecD2 (1/2,000), anti-PpiD (1/20,000
485 or 1/50,000), anti-Ffh (1/10,000) or anti-VemP (1/2,000) antibodies After washing with PBST, the membrane was

incubated with a horseradish peroxidase (HRP)-conjugated secondary antibody (1/5,000) (Goat Anti-Rabbit IgG (H + L)-HRP Conjugate; Bio-Rad Laboratories, Inc., Hercules, CA) in PBST. Proteins were visualized with ECL™ Western Blotting Detection Reagents (GE Healthcare UK Ltd, Amersham Place Little Chalfont, England) or ECL™ Prime Western Blotting Detection Reagents (GE Healthcare) and LAS4000 mini lumino-image analyzer (GE Healthcare).

**PiXie analysis**

This analysis was used in Figures 1B–F, 2A, Figure 1-figure supplements 1A, 2, 3, 4 and Figure 2-figure supplements 1A, C, 2A. Cells were first grown at 30°C in M9-medium supplemented with 2 µg/mL thiamine, 0.4% glycerol, 0.2% maltose, all amino acids (except Met and Cys; final concentration of 20 µg/mL each), 0.5 mM *p*BPA (H-p-Bz-Phe-OH F-2800; Bachem AG, Bubendorf, Switzerland), and 0.02% arabinose until early log phase. After IPTG induction for 15 min, cells were pulse-labeled with 370 kBq/mL [$^{35}$S]Met (American Radiolabeled Chemicals, Inc., St. Louis, MO) for 30 sec. In the case of the experiments in Figure S5A, 0.02% $NaN_3$ and [$^{35}$S]Met were added simultaneously. After addition of excess non-radioactive Met (final conc. 250 µg/mL), a 350 µl portion of the cell cultures was quickly removed and put into wells of a 24-well microtiter plate (AGC Tehcno Glass Co. Ltd, Shizuoka, Japan) on a temperature-controllable and movable stage (MS Tech Co. Ltd., Kyoto, Japan). Cells were kept at 30ºC and UV-irradiated for 1 sec at appropriate time points during chase using SP-9 equipped with an SFH lens (USHIO Inc., Tokyo, Japan) at a distance of 5 cm. Control samples without UV-irradiation in Figure 2A and Figure 1-figure supplement 2A were also put to the microtiter plate on the stage and treated in the same way except that they were not UV-irradiated. After UV irradiation, total cellular proteins were immediately precipitated with 5% trichloroacetic acid (TCA), washed with acetone, and solubilized in SDS-buffer (50 mM Tris-HCl (pH 8.1), 1% SDS, 1 mM EDTA). The samples were then diluted 33-fold with Triton-buffer (50 mM Tris-HCl (pH 8.1), 150 mM NaCl, 2% Triton X-100, 0.1 mM EDTA). After clarification, samples were incubated with appropriate antibodies and nProtein A Sepharose™ 4 Fast Flow (GE healthcare) or Ni-NTA

Agarose (QIAGEN) at 4ºC over-night with slow rotation. Proteins bound to the antibody/ProteinA-Sepharose or Ni-NTA Agarose were recovered by centrifugation, washed with Triton buffer and then with 10 mM Tris-HCl (pH 8.1) and eluted by incubation at 37°C for more than 5 min in SDS-sample buffer (62.5 mM Tris-HCl (pH 6.8), 2% SDS, 10% glycerol, 5 mg/mL bromophenol blue). The isolated proteins were separated by SDS-PAGE, and visualized with BAS1800 phosphoimager (Fujifilm Co., Tokyo, Japan). Band intensities were quantified using MultiGauge software (Fujifilm). To obtain the graphs in Figure 2B, the band intensity of VemP-FL (open diamonds), VemP-APs (AP-un + AP-pro; the signal intensity of the AP-pro is normalized by the Met content) (closed diamonds) and XLs (colored symbols) in Figure 2A was quantitated.

***In vivo* stability of the arrest-form of VemP**

The procedure was used in Figures 3A, 4A, 4D and Figure 5-figure supplement 1B. Cells were first grown at 30°C in M9-medium supplemented with 2 μg/mL thiamine, 0.4% glycerol, 0.2% maltose, all amino acids (except Met and Cys) with or without 0.05% arabinose until early log phase. After induction with for 15 min, cells were pulse-labeled with 370 kBq/mL [$^{35}$S]Met for 30 sec. At appropriate time points after addition of excess nonradioactive Met (final conc. 250 μg/mL), total cellular proteins were precipitated with 5% TCA, washed with acetone, and solubilized in SDS-buffer. The samples were subjected to the IP as described above. Isolated proteins were separated by SDS-PAGE, and visualized with BAS1800 phosphoimager. Percentages of the arrested VemP were calculated by the following equation: arrested VemP (%) = 100 × [VemP-APs ]/[(VemP-FL) + (VemP-APs)], where VemP-APs (in Figure 2B) and VemP-FL are the intensities of the respective bands.

***In vivo* photo-crosslinking analysis**

In the Figure 4E, Cells were grown at 37°C in L medium containing 0.5 mM *p*BPA until early log phase and induced with 0.02% arabinose for 1 h. The half volume of the cell cultures was put on a petri dish at 4ºC and UV-irradiated for 10 min using B-100AP UV lamp (365 nm; UVP, LLC., Upland, CA), at a distance of 4 cm. The

other half was kept on ice as non-UV-irradiated samples. Total cellular proteins were precipitated with 5% TCAs, washed with acetone, and suspended in SDS-sample buffer. The samples were subjected to SDS-PAGE and immunoblotting analysis.

# Article and author information

## Author details

**Ryoji Miyazaki**

Institute for Frontier Life and Medical Sciences, Kyoto University, Kyoto, Japan

**Contribution:** Conceptualization, Methodology, Investigation, Resources, Writing–Original Draft and Funding Acquisition

**Competing interests:** No competing interests declared

**ORCID:** 0000-0003-1626-2569

**Yoshinori Akiyama**

Institute for Frontier Life and Medical Sciences, Kyoto University, Kyoto, Japan

**Contribution:** Writing–Review & Editing, Supervision and Funding Acquisition

**Competing interests:** No competing interests declared

**ORCID:** 0000-0003-4483-5408

**Hiroyuki Mori**

Institute for Frontier Life and Medical Sciences, Kyoto University, Kyoto, Japan

**Contribution:** Conceptualization, Methodology, Investigation, Resources, Writing–Original Draft, Writing–Review & Editing, Supervision and Funding Acquisition

**Competing interests:** No competing interests declared

**ORCID:** 0000-0002-0429-1269

## Funding

This work was supported by the Japan Society for the Promotion of Science KAKENHI Grants 18H06047, 19K21179, 20K15715 (to R.M.), 15H01532, 18H023404 (to Y.A.), and 17H05666, 17H05879, 17K07334, 20K06556 (to H.M.).

## Acknowledgments

We thank Shinobu Chiba, Carol A. Gross and Matthias Müller for providing antibodies, NBRP (NIG, Japan):*E. coli* for bacterial strains, Koreaki Ito for critical reading and editing of the manuscript, and our laboratory members for discussion.

## References


Antonoaea R, Fürst M, Nishiyama K-I, Müller M. 2008. The periplasmic chaperone PpiD interacts with secretory proteins exiting from the SecYEG translocon. *Biochemistry* **47**:5649–5656. doi:10.1021/bi800233w

Baba T, Ara T, Hasegawa M, Takai Y, Okumura Y, Baba M, Datsenko KA, Tomita M, Wanner BL, Mori H. 2006. Construction of *Escherichia coli* K-12 in-frame, single-gene knockout mutants: the Keio collection. *Mol Syst Biol* **2**:2006.0008. doi:10.1038/msb4100050

Baba T, Jacq A, Brickman E, Beckwith J, Taura T, Ueguchi C, Akiyama Y, Ito K. 1990. Characterization of cold-sensitive *secY* mutants of *Escherichia coli*. *J Bacteriol* **172**:7005–7010. doi:10.1128/jb.172.12.7005-7010.1990

Butland G, Peregrín-Alvarez JM, Li J, Yang W, Yang X, Canadien V, Starostine A, Richards D, Beattie B, Krogan N, Davey M, Parkinson J, Greenblatt J, Emili A. 2005. Interaction network containing conserved and essential protein complexes in *Escherichia coli*. *Nature* **433**:531–537. doi:10.1038/nature03239

Chiba S, Lamsa A, Pogliano K. 2009. A ribosome-nascent chain sensor of membrane protein biogenesis in *Bacillus subtilis*. *EMBO J* **28**:3461–3475. doi:10.1038/emboj.2009.280

Chin JW, Martin AB, King DS, Wang L, Schultz PG. 2002. Addition of a photocrosslinking amino acid to the genetic code of *Escherichiacoli*. *Proc Natl Acad Sci U S A* **99**:11020–11024. doi:10.1073/pnas.172226299

Chin JW, Schultz PG. 2002. In vivo photocrosslinking with unnatural amino acid mutagenesis. *Chembiochem* **3**:1135–1137. doi:10.1002/1439-7633(20021104)3:11<1135::AID-CBIC1135>3.0.CO;2-M

Dartigalongue C, Raina S. 1998. A new heat-shock gene, *ppiD*, encodes a peptidyl-prolyl isomerase required for folding of outer membrane proteins in *Escherichia coli*. *EMBO J* **17**:3968–3980. doi:10.1093/emboj/17.14.3968

de Gier JW, Mansournia P, Valent QA, Phillips GJ, Luirink J, von Heijne G. 1996. Assembly of a cytoplasmic membrane protein in *Escherichia coli* is dependent on the signal recognition particle. *FEBS Lett* **399**:307–309. doi:10.1016/s0014-5793(96)01354-3

Economou A, Wickner W. 1994. SecA promotes preprotein translocation by undergoing ATP-driven cycles of membrane insertion and deinsertion. *Cell* **78**:835–843. doi:10.1016/s0092-8674(94)90582-7

Erlandson KJ, Miller SBM, Nam Y, Osborne AR, Zimmer J, Rapoport TA. 2008. A role for the two-helix finger of the SecA ATPase in protein translocation. *Nature* **455**:984–987. doi:10.1038/nature07439

Frauenfeld J, Gumbart J, Sluis EO van der, Funes S, Gartmann M, Beatrix B, Mielke T, Berninghausen O, Becker T, Schulten K, Beckmann R. 2011. Cryo-EM structure of the ribosome-SecYE complex in the membrane environment. *Nat Struct Mol Biol* **18**:614–621. doi:10.1038/nsmb.2026

Fürst M, Zhou Y, Merfort J, Müller M. 2018. Involvement of PpiD in Sec-dependent protein translocation. *Biochim Biophys acta Mol cell Res* **1865**:273–280. doi:10.1016/j.bbamcr.2017.10.012

Furukawa A, Yoshikaie K, Mori T, Mori H, Morimoto Y V, Sugano Y, Iwaki S, Minamino T, Sugita Y, Tanaka Y, Tsukazaki T. 2017. Tunnel formation inferred from the I-form structures of the proton-driven protein secretion motor SecDF. *Cell Rep* **19**:895–901. doi:10.1016/j.celrep.2017.04.030

Huber D, Boyd D, Xia Y, Olma MH, Gerstein M, Beckwith J. 2005. Use of thioredoxin as a reporter to identify a subset of *Escherichia coli* signal sequences that promote signal recognition particle-dependent translocation. *J Bacteriol* **187**:2983–2991. doi:10.1128/JB.187.9.2983-2991.2005

Ishii E, Chiba S, Hashimoto N, Kojima S, Homma M, Ito K, Akiyama Y, Mori H. 2015. Nascent chain-monitored remodeling of the Sec machinery for salinity adaptation of marine bacteria. *Proc Natl Acad Sci U S A* **112**:E5513-22. doi:10.1073/pnas.1513001112

Ito K, Mori H, Chiba S. 2018. Monitoring substrate enables real-time regulation of a protein localization pathway. *FEMS Microbiol Lett* **365**:fny109. doi:10.1093/femsle/fny109

Justice SS, Hunstad DA, Harper JR, Duguay AR, Pinkner JS, Bann J, Frieden C, Silhavy TJ, Hultgren SJ. 2005. Periplasmic peptidyl prolyl *cis-trans* isomerases are not essential for viability, but SurA is required for pilus biogenesis in *Escherichia coli*. *J Bacteriol* **187**:7680–7686. doi:10.1128/JB.187.22.7680-7686.2005

Kramer G, Shiber A, Bukau B. 2019. Mechanisms of cotranslational maturation of newly synthesized proteins. *Annu Rev Biochem* **88**:337–364. doi:10.1146/annurev-biochem-013118-111717

Kuhn A, Koch H-G, Dalbey RE. 2017. Targeting and insertion of membrane proteins. *EcoSal Plus* **7**:doi:10.1128/ecosalplus.ESP-0012-2016. doi:10.1128/ecosalplus.ESP-0012-2016

Kuhn P, Weiche B, Sturm L, Sommer E, Drepper F, Warscheid B, Sourjik V, Koch H-G. 2011. The bacterial SRP receptor, SecA and the ribosome use overlapping binding sites on the SecY translocon. *Traffic* **12**:563–578. doi:10.1111/j.1600-0854.2011.01167.x

Lill R, Cunningham K, Brundage LA, Ito K, Oliver D, Wickner W. 1989. SecA protein hydrolyzes ATP and is an essential component of the protein translocation ATPase of *Escherichia coli*. *EMBO J* **8**:961–966.

Matern Y, Barion B, Behrens-Kneip S. 2010. PpiD is a player in the network of periplasmic chaperones in *Escherichia coli*. *BMC Microbiol* **10**:251. doi:10.1186/1471-2180-10-251

Matsuyama S, Fujita Y, Mizushima S. 1993. SecD is involved in the release of translocated secretory proteins from the cytoplasmic membrane of *Escherichia coli*. *EMBO J* **12**:265–270.

Miller JH. 1972. Experiments in Molecular Genetics. Cold Spring Harbor Laboratory Press.

Miyazaki R, Akiyama Y, Mori H. 2020. A photo-cross-linking approach to monitor protein dynamics in living cells. *Biochim Biophys Acta Gen Subj* **1864**:129317. doi:10.1016/j.bbagen.2019.03.003

Miyazaki R, Myougo N, Mori H, Akiyama Y. 2018. A photo-cross-linking approach to monitor folding and assembly of newly synthesized proteins in a living cell. *J Biol Chem* **293**:677–686. doi:10.1074/jbc.M117.817270

Miyazaki R, Yura T, Suzuki T, Dohmae N, Mori H, Akiyama Y. 2016. A novel SRP recognition sequence in the homeostatic control region of heat shock transcription factor $\sigma^{32}$. *Sci Rep* **6**:24147. doi:10.1038/srep24147

Mori H, Ito K. 2006a. Different modes of SecY-SecA interactions revealed by site-directed *in vivo* photo-cross-linking. *Proc Natl Acad Sci U S A* **103**:16159–16164. doi:10.1073/pnas.0606390103

Mori H, Ito K. 2006b. The long α-helix of SecA is important for the ATPase coupling of translocation. *J Biol Chem* **281**:36249–36256. doi:10.1074/jbc.M606906200

Mori H, Ito K. 2001. The Sec protein-translocation pathway. *Trends Microbiol* **9**:494–500. doi:10.1016/s0966-842x(01)02174-6

Mori H, Sakashita S, Ito J, Ishii E, Akiyama Y. 2018. Identification and characterization of a translation arrest motif in VemP by systematic mutational analysis. *J Biol Chem* **293**:2915–2926. doi:10.1074/jbc.M117.816561

Nakamori K, Chiba S, Ito K. 2014. Identification of a SecM segment required for export-coupled release from elongation arrest. *FEBS Lett* **588**:3098–3103. doi:10.1016/j.febslet.2014.06.038

649 Nakatogawa H, Ito K. 2002. The ribosomal exit tunnel functions as a discriminating gate. *Cell* **108**:629–636.
650 doi:10.1016/s0092-8674(02)00649-9
651 Nakatogawa H, Ito K. 2001. Secretion monitor, SecM, undergoes self-translation arrest in the cytosol. *Mol Cell*
652 **7**:185–192. doi:10.1016/s1097-2765(01)00166-6
653 Nishiyama K, Hanada M, Tokuda H. 1994. Disruption of the gene encoding p12 (SecG) reveals the direct
654 involvement and important function of SecG in the protein translocation of *Escherichia coli* at low
655 temperature. *EMBO J* **13**:3272–3277.
656 Nishiyama K, Mizushima S, Tokuda H. 1993. A novel membrane protein involved in protein translocation across
657 the cytoplasmic membrane of *Escherichia coli. EMBO J* **12**:3409–3415.
658 Oliver DB, Beckwith J. 1982. Regulation of a membrane component required for protein secretion in *Escherichia*
659 *coli*. *Cell* **30**:311–319. doi:10.1016/0092-8674(82)90037-x
660 Pechmann S, Willmund F, Frydman J. 2013. The ribosome as a hub for protein quality control. *Mol Cell* **49**:411–
661 421. doi:10.1016/j.molcel.2013.01.020
662 Pogliano JA, Beckwith J. 1994. SecD and SecF facilitate protein export in *Escherichia coli*. *EMBO J* **13**:554–561.
663 Rapoport TA, Li L, Park E. 2017. Structural and mechanistic insights into protein translocation. *Annu Rev Cell*
664 *Dev Biol* **33**:369–390. doi:10.1146/annurev-cellbio-100616-060439
665 Rubio A, Jiang X, Pogliano K. 2005. Localization of translocation complex components in *Bacillus subtilis*:
666 enrichment of the signal recognition particle receptor at early sporulation septa. *J Bacteriol* **187**:5000–5002.
667 doi:10.1128/JB.187.14.5000-5002.2005
668 Sachelaru I, Petriman N-A, Kudva R, Koch H-G. 2014. Dynamic interaction of the Sec translocon with the
669 chaperone PpiD. *J Biol Chem* **289**:21706–21715. doi:10.1074/jbc.M114.577916
670 Shimohata N, Akiyama Y, Ito K. 2005. Peculiar properties of DsbA in its export across the *Escherichia coli*
671 cytoplasmic membrane. *J Bacteriol* **187**:3997–4004. doi:10.1128/JB.187.12.3997-4004.2005
672 Steinberg R, Knüpffer L, Origi A, Asti R, Koch H-G. 2018. Co-translational protein targeting in bacteria. *FEMS*
673 *Microbiol Lett* **365**:fny095. doi:10.1093/femsle/fny095
674 Su T, Cheng J, Sohmen D, Hedman R, Berninghausen O, von Heijne G, Wilson DN, Beckmann R. 2017. The
675 force-sensing peptide VemP employs extreme compaction and secondary structure formation to induce
676 ribosomal stalling. *eLife* **6**:e25642. doi:10.7554/eLife.25642
677 Tanaka Y, Sugano Y, Takemoto M, Mori T, Furukawa A, Kusakizako T, Kumazaki K, Kashima A, Ishitani R,
678 Sugita Y, Nureki O, Tsukazaki T. 2015. Crystal structures of SecYEG in lipidic cubic phase elucidate a
679 precise resting and a peptide-bound state. *Cell Rep* **13**:1561–1568. doi:10.1016/j.celrep.2015.10.025
680 Taura T, Baba T, Akiyama Y, Ito K. 1993. Determinants of the quantity of the stable SecY complex in the
681 *Escherichia coli* cell. *J Bacteriol* **175**:7771–7775. doi:10.1128/jb.175.24.7771-7775.1993
682 Tenson T, Ehrenberg M. 2002. Regulatory nascent peptides in the ribosomal tunnel. *Cell* **108**:591–594.
683 doi:10.1016/s0092-8674(02)00669-4
684 Terashima H, Koike M, Kojima S, Homma M. 2010. The flagellar basal body-associated protein FlgT is essential
685 for a novel ring structure in the sodium-driven *Vibrio* motor. *J Bacteriol* **192**:5609–5615.
686 doi:10.1128/JB.00720-10
687 Tsukazaki T. 2018. Structure-based working model of SecDF, a proton-driven bacterial protein translocation factor.
688 *FEMS Microbiol Lett* **365**:fny112. doi:10.1093/femsle/fny112

689 Tsukazaki T, Mori H, Echizen Y, Ishitani R, Fukai S, Tanaka T, Perederina A, Vassylyev DG, Kohno T, Maturana
690 AD, Ito K, Nureki O. 2011. Structure and function of a membrane component SecDF that enhances protein
691 export. *Nature* **474**:235–238. doi:10.1038/nature09980
692 Van den Berg B, Clemons WMJ, Collinson I, Modis Y, Hartmann E, Harrison SC, Rapoport TA. 2004. X-ray
693 structure of a protein-conducting channel. *Nature* **427**:36–44. doi:10.1038/nature02218
694 Yanagitani K, Kimata Y, Kadokura H, Kohno K. 2011. Translational pausing ensures membrane targeting and
695 cytoplasmic splicing of XBP1u mRNA. *Science* **331**:586–589. doi:10.1126/science.1197142
696 Yap M-N, Bernstein HD. 2011. The translational regulatory function of SecM requires the precise timing of
697 membrane targeting. *Mol Microbiol* **81**:540–553. doi:10.1111/j.1365-2958.2011.07713.x
698 Yu D, Ellis HM, Lee EC, Jenkins NA, Copeland NG, Court DL. 2000. An efficient recombination system for
699 chromosome engineering in *Escherichia coli*. *Proc Natl Acad Sci U S A* **97**:5978–5983.
700 doi:10.1073/pnas.100127597
701 Zimmer J, Nam Y, Rapoport TA. 2008. Structure of a complex of the ATPase SecA and the protein-translocation
702 channel. *Nature* **455**:936–943. doi:10.1038/nature07335
703
704

## List of Figure supplements.

**Figure 1-figure supplement 1 Systematic PiXie analysis of a nascent VemP**

**Figure 1-figure supplement 2 Identification of VemP crosslinked products**

**Figure 1-figure supplement 3 Identification of VemP crosslinked products using His-tagged derivatives of candidate proteins**

**Figure 1-figure supplement 4 Immunoprecipitation of VemP-crosslinked products using anti-FLAG antibodies**

**Figure 2-figure supplement 1 PiXie analysis of VemP interactions**

**Figure 2-figure supplement 2 Effect of $NaN_3$ treatment on VemP crosslinking**

**Figure 5-figure supplement 1 The conserved Arg-85 residue is important for the stability of an arrested VemP *in vivo***

**Figure 5-figure supplement 2 Sequence alignment of VemP orthologues**

## List of Supplementary files

**Supplementary file 1: Table S1. Strains used in this study**

**Supplementary file 2: Table S2. Plasmids used in this study**

**Supplementary file 3: Table S3. Primers used in this study**

# Figure 1

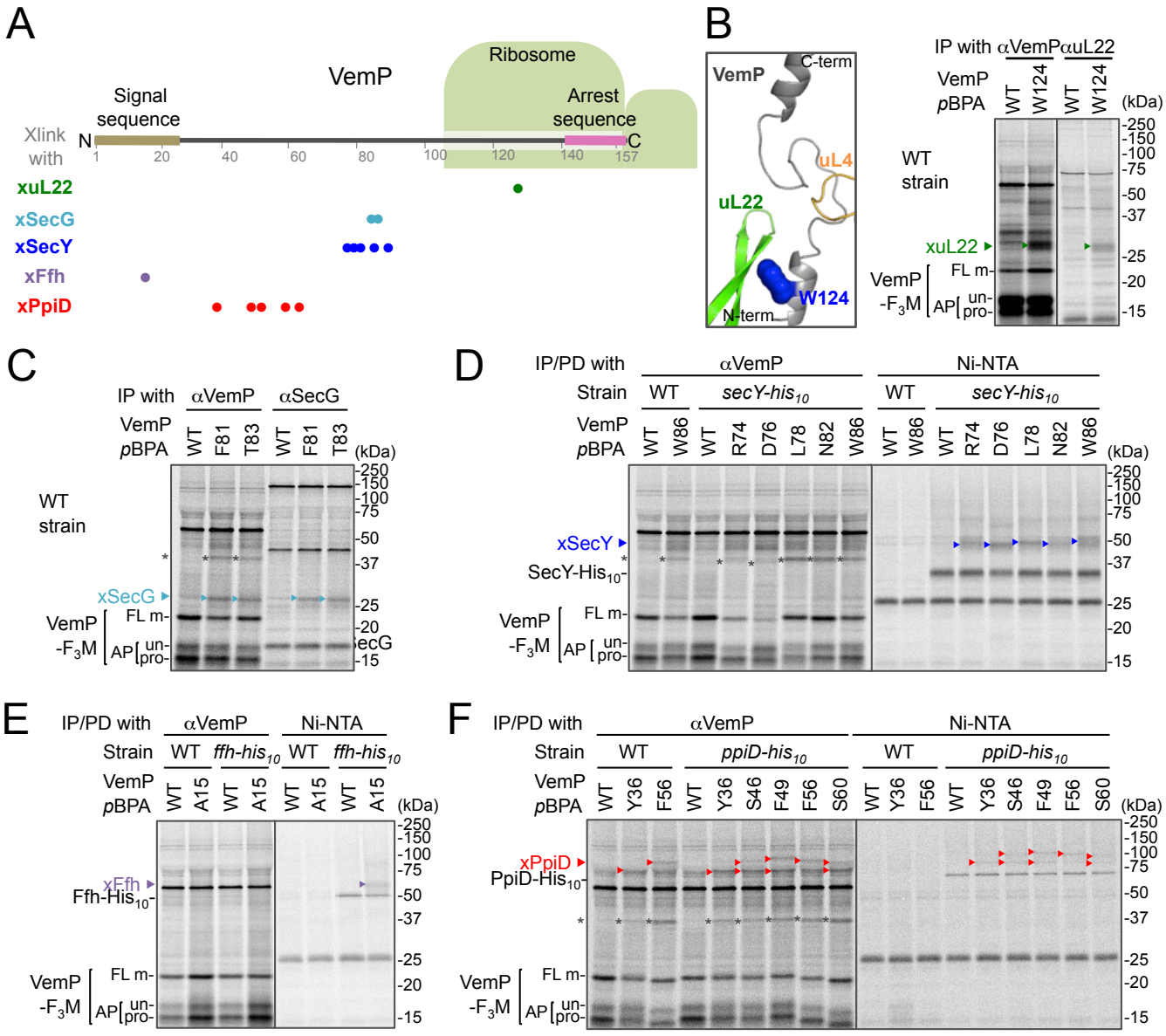


**Figure 1.** ***In vivo*** **crosslinking reveals interaction of a VemP nascent polypeptide with Ffh and PpiD as well as uL22 and translocon**

(**A**) Summary of proteins crosslinked with VemP in the arrested state. Colored circles represent the positions at which crosslinking with the indicated proteins was observed. (**B-F**) PiXie analysis of VemP. Wild type *E.coli* cells were used in **B** and **C**. *E. coli* cells expressing SecY-$His_{10}$, Ffh-$His_{10}$, or PpiD-$His_{10}$ from the chromosome were used in **D, E** and **F**, respectively. Wild type cells were used as negative controls in **D**, **E** and **F**. Cells were grown, induced to express a VemP-$F_3M$ derivative and pulse-labeled with [$^{35}$S]Met for 30 sec, followed by 30 sec-chase as described in Materials and Methods. Cells were UV irradiated for 1 sec and immediately acid-treated. Labeled proteins were subjected to immunoprecipitation (IP) or pull-down (PD) with Ni-NTA agarose, separated by SDS-PAGE and analyzed by phosphorimaging. The results shown are representatives of two independent experiments that were conducted using the same transformants (i.e. two technical replicates). Asterisks represent crosslinked dimers of VemP-$F_3M$. An enlarged view around Trp-124 of VemP in a VemP-stalled ribosome complex (PDB:5nwy; Su et al., 2017) is shown in **B**, *left*.

# Figure 2

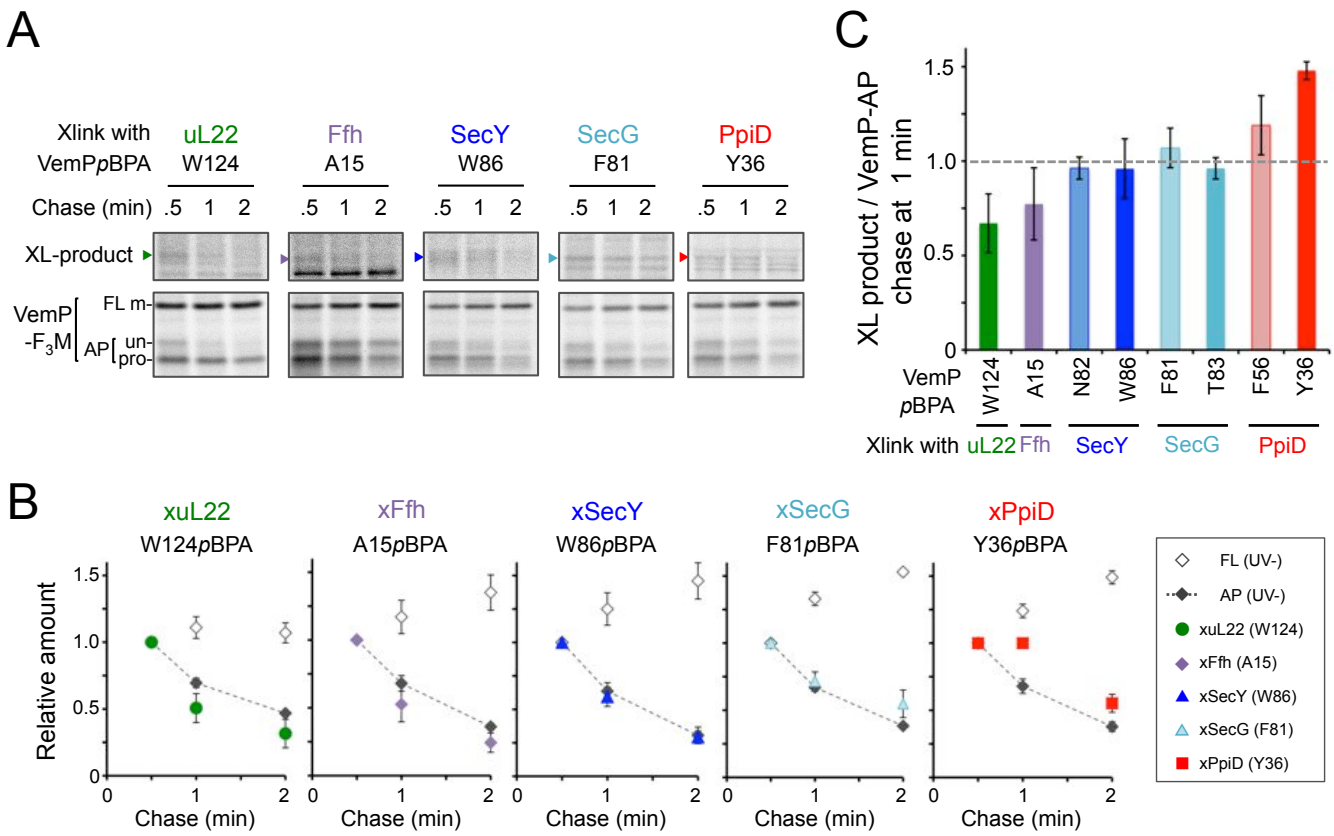


**Figure 2. The VemP nascent polypeptide interacts sequentially with uL22/Ffh, the translocon, and PpiD**
(**A**) PiXie analysis of VemP. Cells were grown, induced to express a VemP derivative with *p*BPA, pulse-labeled and chased as in Figure 1. At the indicated time points in the chase period, cells were UV-irradiated for 1 sec and then acid-treated. Labeled proteins were subjected to IP with an anti-VemP antibody or pull-down with Ni-NTA agarose. The same strains were parallelly pulse-labeled, chased, and subjected to IP with the anti-VemP antibody without the UV irradiation. Isolated proteins were analyzed as in Figure 1. Portions of the gel images showing the XLs (*upper gels*) or showing the VemP-derived bands of the UV-unirradiated samples (*lower gels*) are presented. The results shown are representatives of three technical replicates. (**B**) Relative amounts of the VemP arrested forms and the VemP-XLs. The band intensity of VemP-FL (open diamonds), VemP-APs (AP-un + AP-pro) (closed diamonds) and XLs (colored symbols) in **A** was quantitated and the mean values of the relative values (the value at the 0.5 min was set to 1) were plotted (error bars are S.D.; (n = 3)). (**C**) Relative crosslinking efficiency of the arrested VemP. The values for the relative intensities of XLs at 1min to the corresponding average intensities of VemP-APs were calculated from the results in Figures 2B and Figure2-figure supplement 1B, D. The mean values are shown with S.D. (n = 3 technical replicates).

# Figure 3

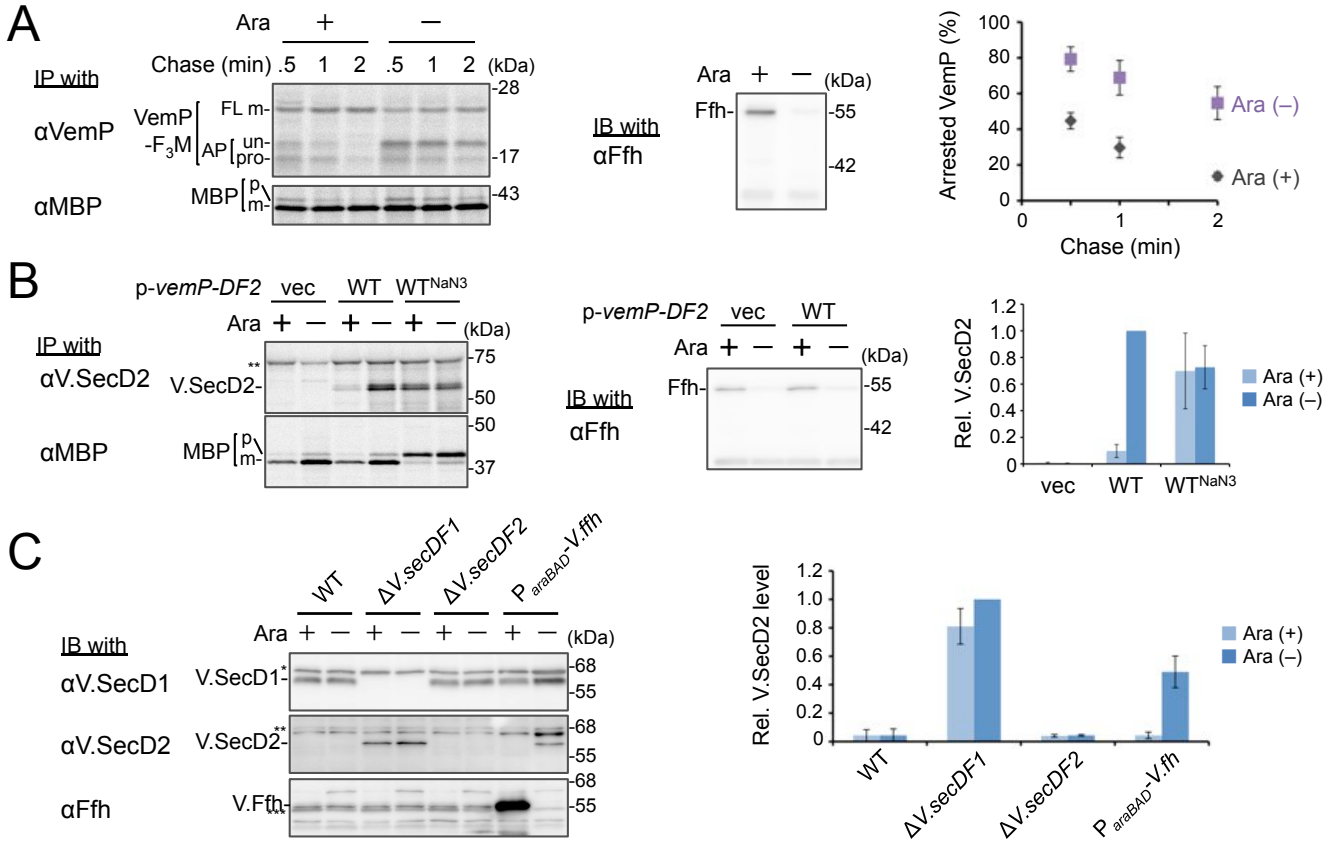


**Figure 3. Ffh (SRP) functions in the targeting of VemP**

(**A**) Effects of Ffh-depletion on stability of the arrested-VemP. (***left***) Ffh-depletable cells carrying a *vemP-f*$_3$*m* plasmid were grown in the M9 medium with (+) or without (–) 0.05% arabinose, induced, pulse-labeled and chased as in Figure 1**.** At the indicated chase time points, total cellular proteins were acid-precipitated, subjected to IP and analyzed as in Figure 1. (***middle***) In parallel, a portion of the cultures just before pulse-labeling was subjected to immunoblotting (IB) analysis with an anti-Ffh antibody. (***right***) Percentages of the arrested VemP in ***left*** were calculated by the equation described in Materials and Methods. Values are means ± S.D. (n = 3 technical replicates). (**B**) Effects of Ffh-depletion on the expression of *V.secD2*. (***left***) The Ffh-depletable cells carrying an empty vector or a *vemP-V.secD2/F2* plasmid (WT) were grown, induced and pulse-labeled for 1 min. Total cellular proteins were acid-precipitated. For the WT$^{NaN3}$ samples, the cells carrying the *vemP-V.secD2/F2* plasmid were pretreated with 0.02% $NaN_3$ for 5 min before pulse-labeling. Labeled proteins were subjected to IP, and analyzed as in Figure 1. (***middle***) In parallel, a portion of the cultures just before the pulse-labeling was subjected to IB with the anti-Ffh antibody. The intensity of the V.SecD2 band from each lane was quantitated. Values are means ± S.D. (n = 3 technical replicates) (the value for WT in the presence of arabinose was set to 1). (**C**) Effects of Ffh-depletion on the expression of *V.secD2* in a *Vibrio* cell. (***left***) The *Vibrio* cells indicated were grown at 30˚C in VC-medium with (+) or without (–) 0.2% arabinose for 3 h. Total cellular proteins were acid-precipitated, and analyzed by IB. (***right***) The intensity of the V.SecD2 band from each lane was quantitated. Values are means ± S.D. (n = 3 technical replicates) (the value for the D*V.secD1* cells in the presence of arabinose was set to 1). The asterisks (*, **, ***) in **B** and, **C** represent un-related proteins recognized by the indicated antibodies.

# Figure 4

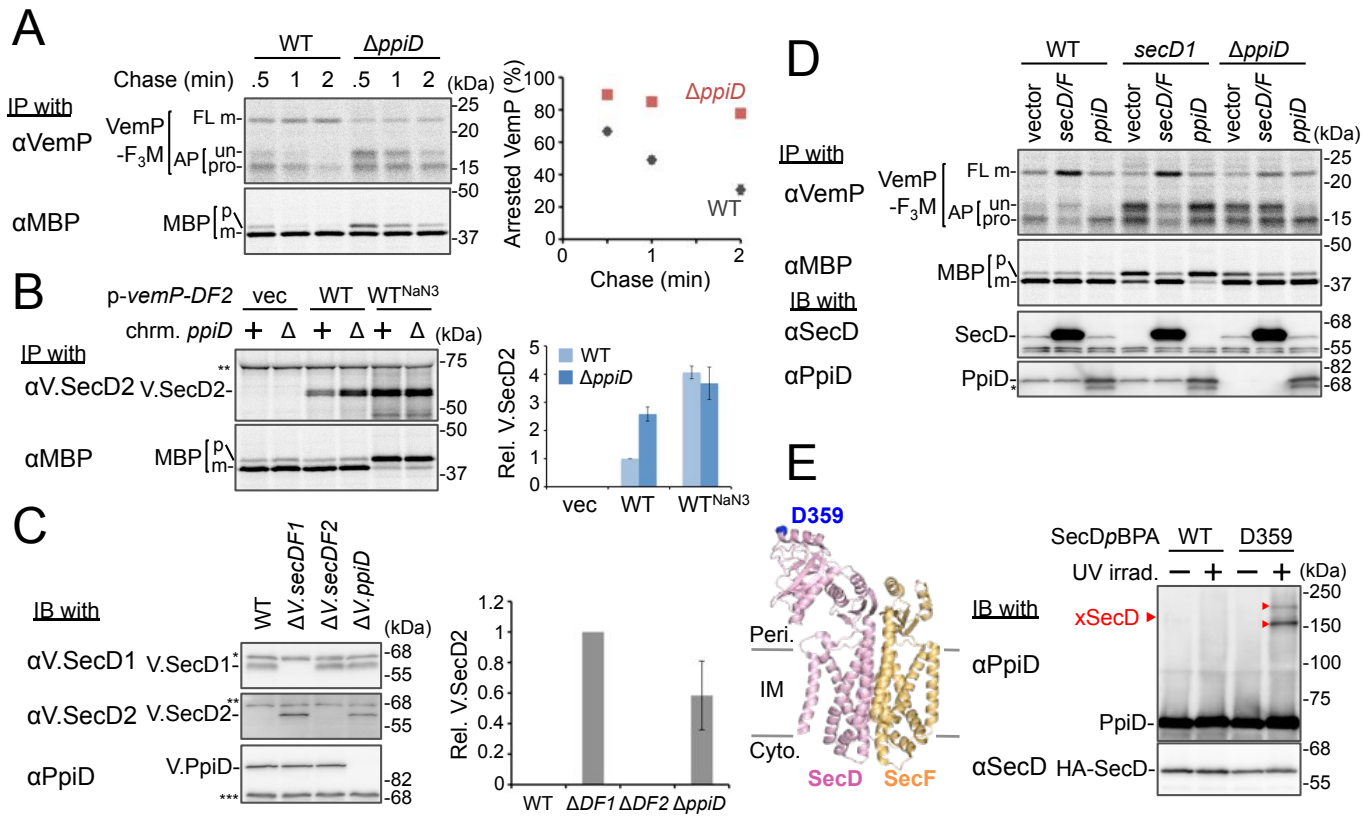


**Figure 4. PpiD and SecD/F cooperate to facilitate the translocation and the arrest cancelation of VemP**

(**A**) Effects of the *ppiD* disruption on the stability of the arrested-VemP. (***left***) WT cells or Δ*ppiD* cells carrying the *vemP-f$_3$m* plasmid were grown, induced, pulse-labeled and chased as in Figure 1. At the indicated chase time points, total cellular proteins were acid-precipitated and subjected to IP and analyzed as in Figure 1. (***right***) The mean values of arrested VemP (%) are plotted with S.D. (n = 3 technical replicates). (**B**) Effects of the *ppiD* disruption on the expression of *V.secD2*. (***left***) WT cells or Δ*ppiD* cells carrying either an empty vector or a *vemP-V.secD2/F2* plasmid (WT) were grown, induced as in **A** and pulse-labeled for 1 min. For the WT$^{NaN3}$ samples, the cells carrying the *vemP-V.secD2/F2* plasmid were pretreated with 0.02% $NaN_3$ for 5 min before pulse-labeling. Labeled proteins were subjected to IP and analyzed as in Figure 1. The intensities of the V.SecD2 bands were quantitated. Values are means ± S.D. (n = 3 technical replicates) (the value for the WT cells was set to 1). (**C**) Effects of the *ppiD* disruption on the expression of *V.secD2* in *Vibrio* cells. (***left***) The indicated *Vibrio* cells were grown at 30˚C in the VC-medium for 2 h. Total cellular proteins were acid-precipitated and subjected to IB. (***right***) The intensities of the V.SecD2 bands were quantitated. Values are means ± S.D. (n = 3 technical replicates) (the value for the D*secD1* cells was set to 1). The asterisks (*, **, ***) in **B** and **C** represent un-related proteins recognized by the indicated antibodies. (**D**) Roles of SecD/F and PpiD in the arrest-release of VemP. A pRM83c-based plasmid carrying either *his$_{10}$-secD/F* or *ppiD,* or the empty vector was introduced, in addition to pHM1021-*vemP-f$_3$m,* into wild type cells and cells having either the *secD1* or the Δ*ppiD* mutation. These cells were grown at 37˚C for 2.5 h as in Figure 1. A half of the cell cultures were removed and acid-treated. Precipitated proteins were subjected to IB (*lower two panels*). The remaining cells were induced with 1 mM IPTG for 15 min, pulse-labeled for 30 sec and chased for 30 sec. Acid-precipitated proteins were subjected to IP and analyzed as in Figure 1 (*upper two panels*). The results shown are representatives of two technical replicates. The asterisk in the lowest gel represents a degradation product of PpiD. (**E**) *In vivo* photo-crosslinking of SecD with PpiD. Cells were grown in L medium containing 0.5 mM *p*BPA until early log phase at 37˚C and induced with 0.02% arabinose for 1 h to express the indicated SecD/F variants. The cultures were divided into two portions, each of which was treated with or without UV-irradiation for 10 min at 4˚C. Total cellular proteins were acid-precipitated and subjected to IB. The result shown is a representative of two technical replicates. A crystal structure of SecD/F (PDB:3aqp; Tsukazaki et al., 2011) is shown in the left.

# Figure 5

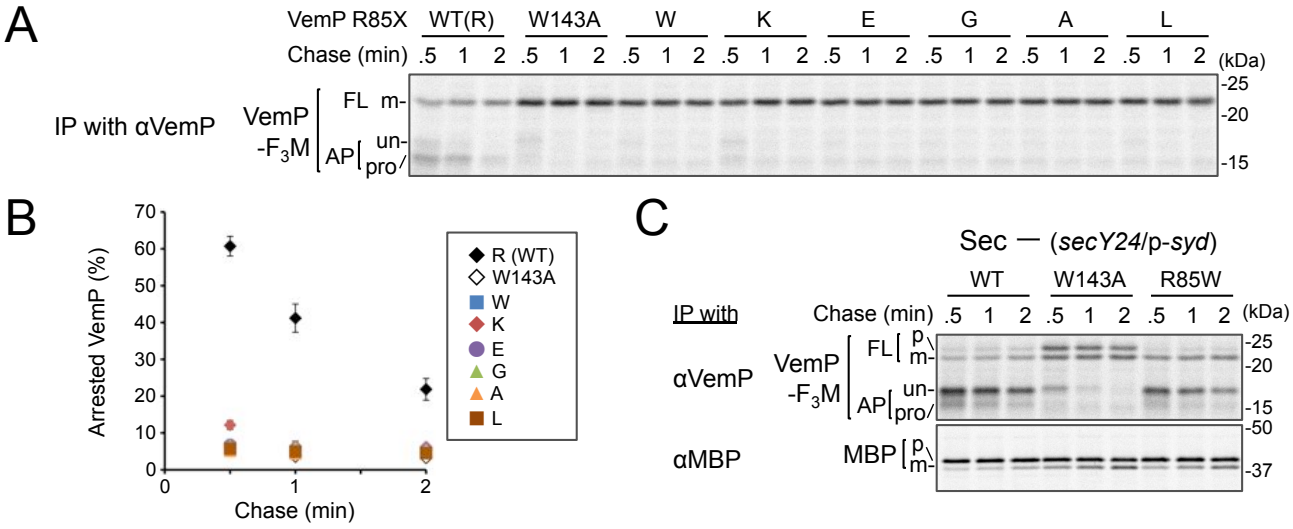


**Figure 5. Conserved Arg-85 has a role in the regulation of secretion-coupling of the VemP arrest cancelation**
(**A, B**) Effects of Arg-85 mutations on the stability of the arrested VemP *in vivo*. Cells were grown, induced to express the indicated VemP-$F_3$M derivatives, and used for the pulse-chase experiments as in Figure 4A. Labeled proteins were subjected to IP with an anti-VemP antibody and analyzed as in Figure 1. The mean values of the arrested VemP (%) are plotted with S.D. (n ≥ 3 technical replicates) in **B**. (**C**) Behavior of the VemP(R85W) mutant under Sec-deficient conditions. Cells defective in protein translocation (*secY24*/pSTV28-*syd*) expressing the indicated VemP-$F_3$M derivatives were examined by the pulse-chase experiment as described in Figure 4A except that the export of MBP was also examined by IP with an anti-MBP antibody. The results shown are representatives of two technical replicates.

# Figure 6

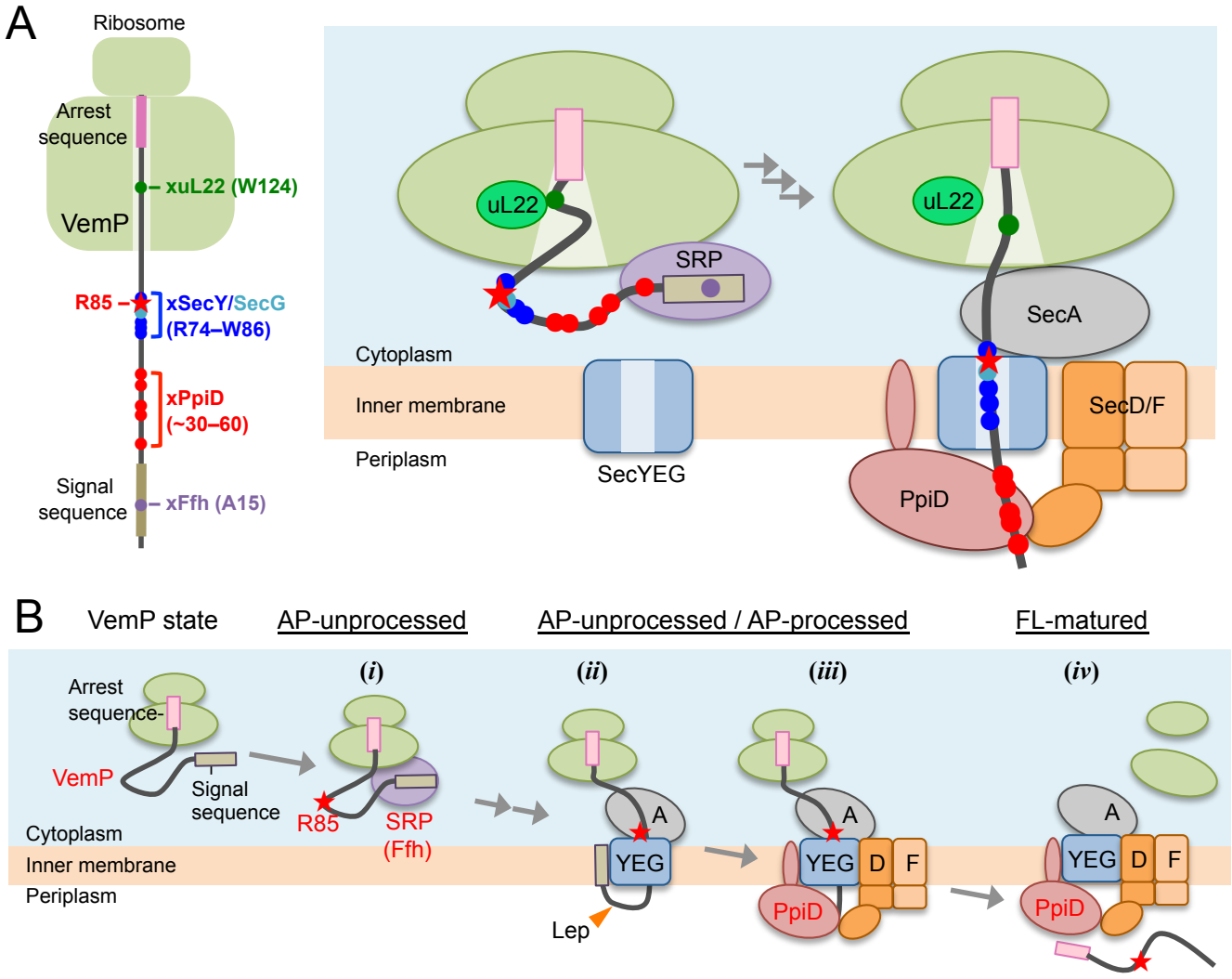


**Figure 6. A model of the arrest-cancelation of a VemP nascent polypeptide**

(**A**) Schematic interaction maps of VemP during its translocation processes. The positions of the crosslinking with other factors and Arg-85 are mapped on the schematic picture of the arrested VemP-ribosome complex (***left***). Hypothetical models of the nascent VemP-ribosome complex on the Sec machinery (***right***). See the text for details. (**B**) An overview of the translocation processes of the arrested VemP including the arrest-cancelation steps. See the text for details.

# Figure 1-figure supplement 1

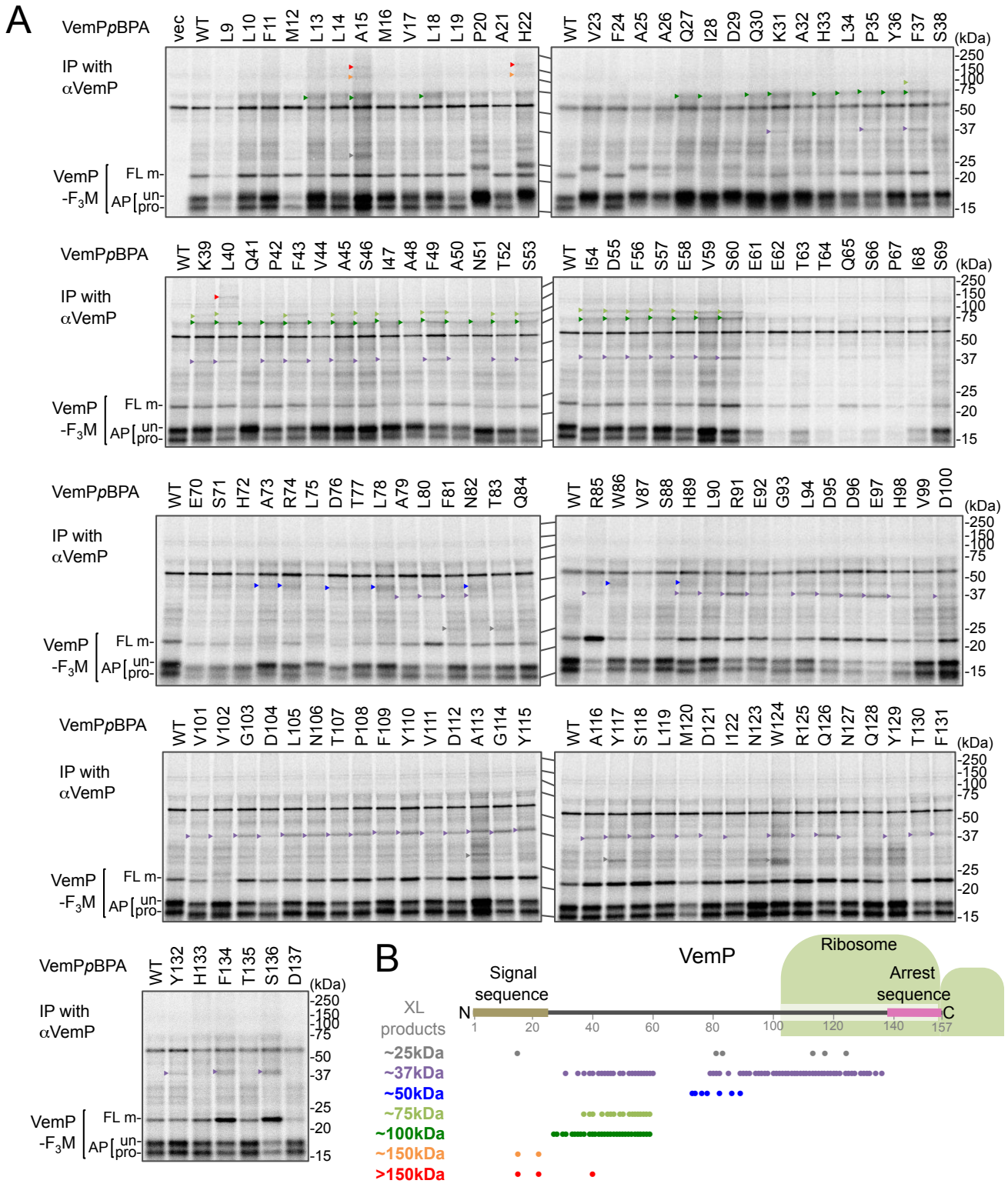


**Figure 1-figure supplement 1 Systematic PiXie analysis of a nascent VemP**

(**A**) Systematic PiXie analysis of VemP. Cells were grown as described in Materials and Methods, induced with 1 mM IPTG for 15 min to express VemP-$F_3$M derivatives with *p*BPA at the indicated position, pulse-labeled with [$^{35}$S]Met for 30 sec, and chased for 30 sec with excess unlabeled Met. The cells were then UV-irradiated for 1 sec. Total cellular proteins were acid-precipitated and subjected to immunoprecipitation (IP) with an anti-VemP antibody. Immuno-isolated proteins were separated by SDS-PAGE and analyzed by phosphorimaging. The results shown are representatives of two technical replicates. Crosslinked products (XLs) that are classified from their apparent sizes are marked by arrowheads with different colors. (**B**) Summary of the crosslinked proteins and their positions of crosslinking. A schematic picture of the VemP polypeptide in the arrested state is presented with the residue numbers. The positions of the crosslinking to each protein are represented as circles with the same colors as in **A**.

# Figure 1-figure supplement 2

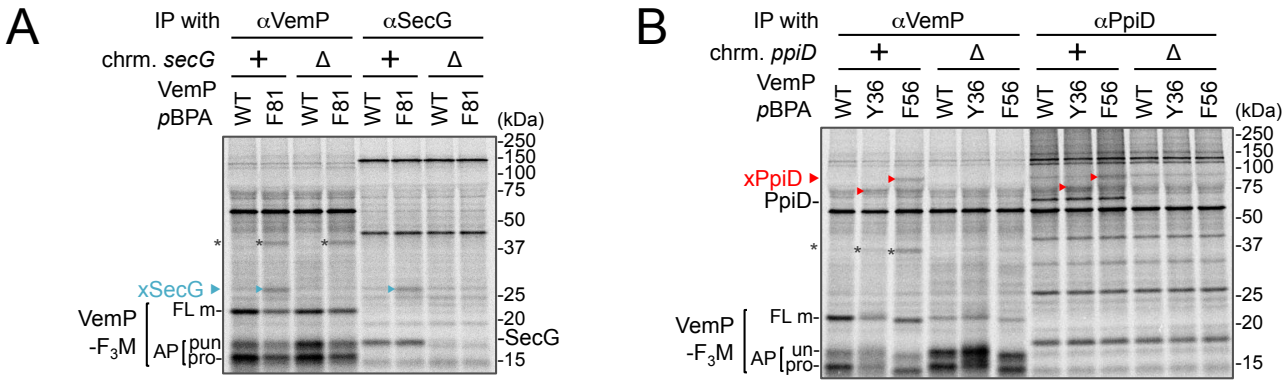


**Figure 1-figure supplement 2 Identification of VemP crosslinked products**

(**A**) VemPxSecG XLs. (**B**) VemPxPpiD XLs. The cells of the indicated strains were grown, induced to express a VemP-$F_3$M derivative with *p*BPA at the indicated position (WT indicates the protein with no *p*BPA), pulse-chased, and UV irradiated as in Figure 1. Labeled proteins were subjected to IP with indicated antibodies and analyzed as in Figure 1. The results shown are representatives of two technical replicates. Asterisks in **A** and **B** represent crosslinked dimer forms of VemP-$F_3$M.

# Figure 1-figure supplement 3

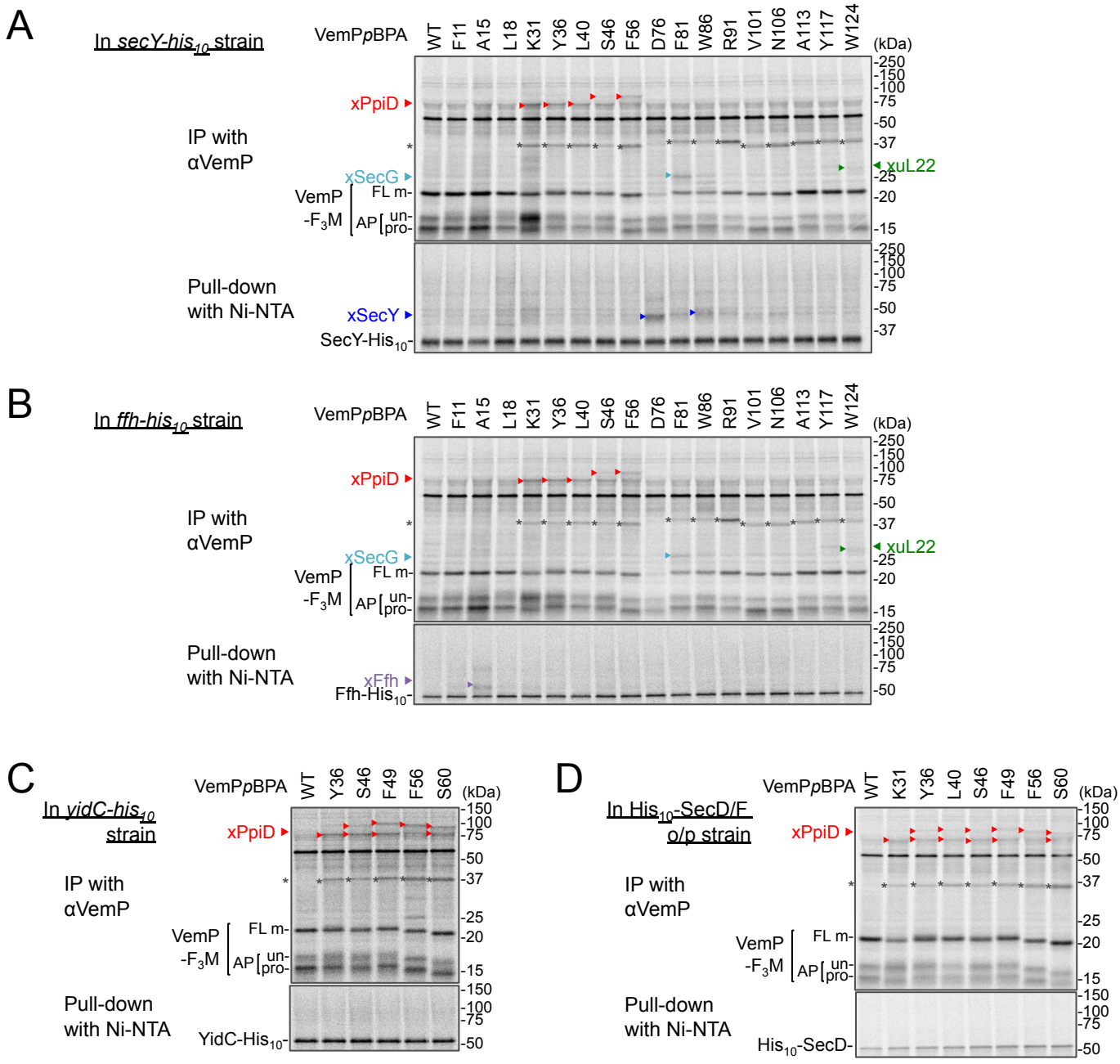


**Figure 1-figure supplement 3 Identification of VemP crosslinked products using His-tagged derivatives of candidate proteins**
(**A–D**) VemP PiXie analysis in cells expressing $His_{10}$-tagged proteins. *E. coli* strains, RM2834 (expressing SecY-$His_{10}$ from the chromosome, **A**), RM2831 (Ffh-$His_{10}$, **B**), and RM2935 (YidC-$His_{10}$, **C**) were constructed (See Materials and Methods) and used. The cells of the indicated strains were grown, induced to express a VemP-$F_3$M derivative with *p*BPA at the indicated position and analyzed by the PiXie methods as described in Figure 1. Labeled proteins were subjected to IP with an anti-VemP antibody (***upper gel***) or pull-down with Ni-NTA agarose (***lower gel***). Immuno-isolated proteins were analyzed as in Figure 1. (**D**) *secD1* mutant cells over-expressing $His_{10}$-SecD/F were grown and induced to express a VemP-$F_3$M derivative with *p*BPA at the indicated position and analyzed by PiXie as in Figure 1. Labeled proteins were subjected to IP with the anti-VemP antibody (***upper gel***) or pull-down with Ni-NTA agarose (***lower gel***). Immuno-isolated proteins were analyzed as in Figure 1. The results shown are representatives of two technical replicates. Asterisks in **A–D** represent crosslinked dimer forms of VemP-$F_3$M.

# Figure 1-figure supplement 4

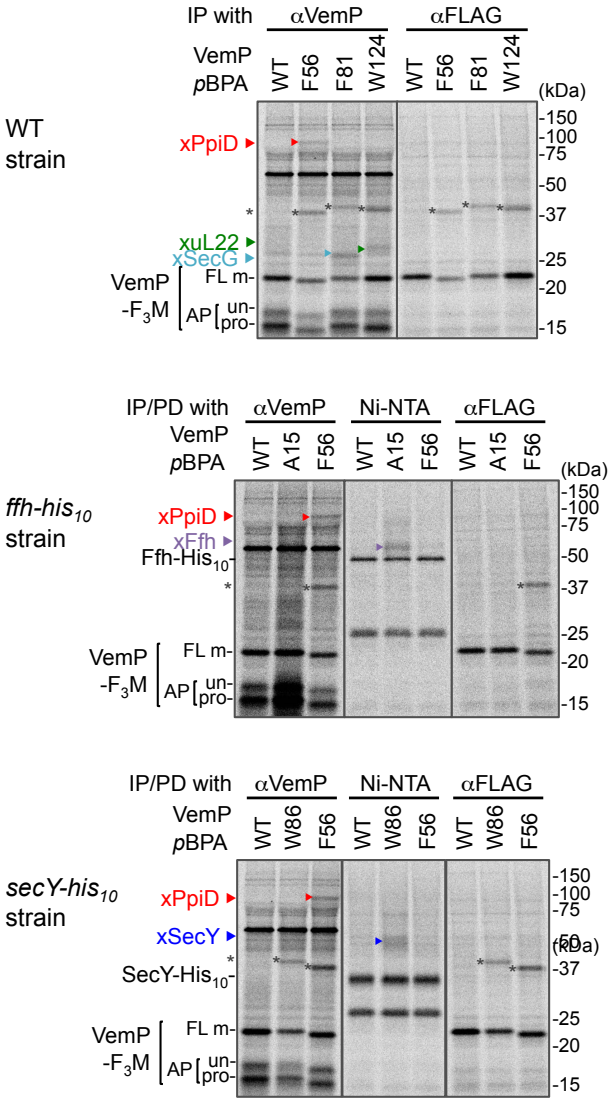


**Figure 1-figure supplement 4 Immunoprecipitation of VemP-crosslinked products using anti-FLAG antibodies**
The cells of the indicated strains were grown, induced to express a VemP-$F_3$M derivative with *p*BPA at the indicated position (WT indicates the protein with no *p*BPA), and analyzed by PiXie as in Figure 1. Labeled proteins were subjected to IP with the indicated antibodies or pull-down with Ni-NTA agarose. Immuno-isolated proteins were analyzed as in Figure **1**. The results shown are representatives of two technical replicates. The VemP XLs with PpiD, uL22, SecG, SecY-$His_{10}$, and Ffh-$His_{10}$ are marked by triangles colored in red, green, pale blue, blue, and violet, respectively. Asterisks presumably represent crosslinked dimer forms of full-length VemP-$F_3$M.

# Figure 2-figure supplement 1

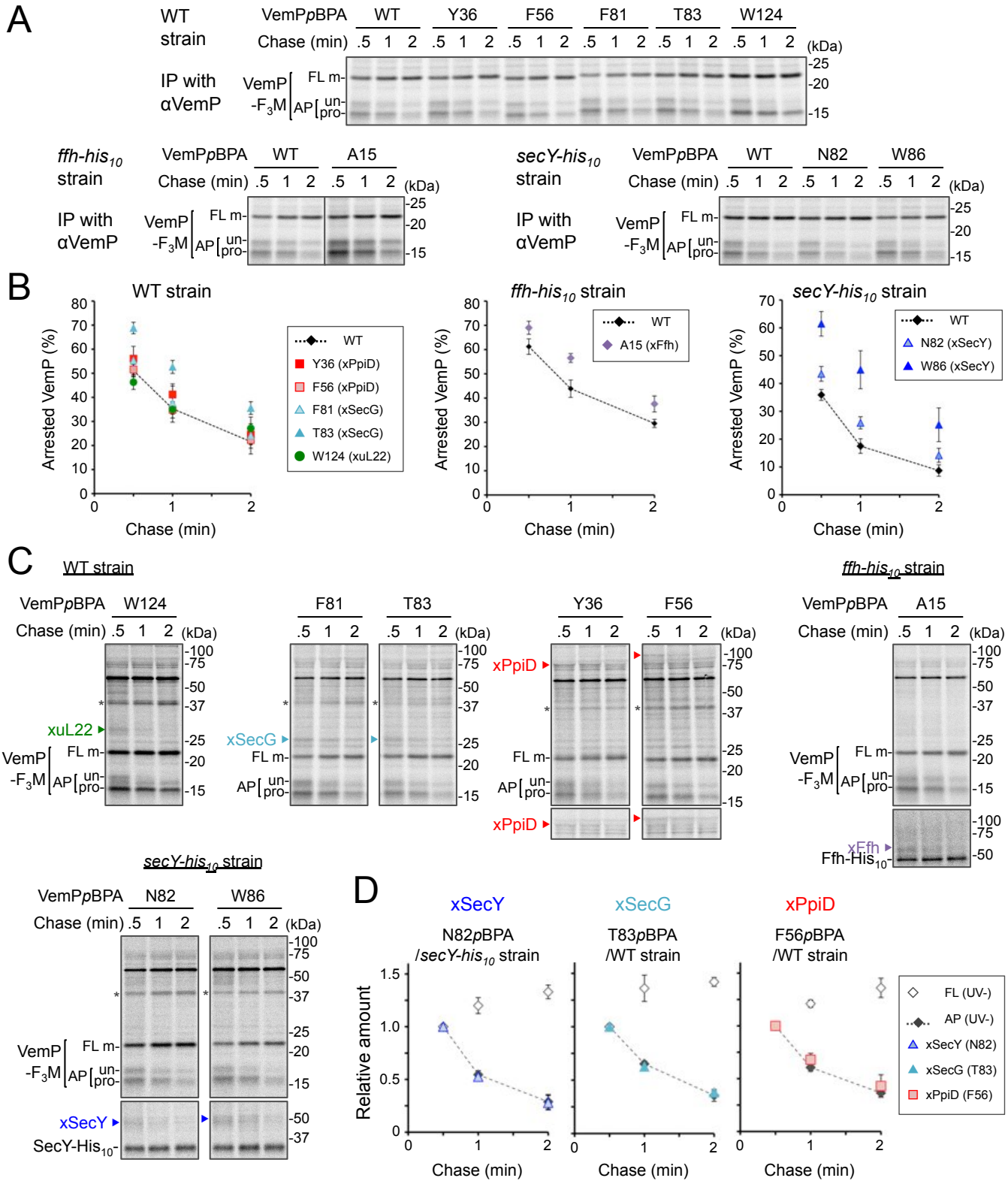


**Figure 2-figure supplement 1 PiXie analysis of VemP interactions**

(**A, B**) Stability of the arrested form of the VemP*p*BPA derivatives. Cells were grown, induced to express a VemP-$F_3$M derivative with *p*BPA at the indicated position (WT indicates the protein with no *p*BPA), pulse-labeled and chased as described in Figure. 4A. Labeled proteins were subjected to IP with anti-VemP antibodies and analyzed as in Figure 1. Arrested VemP (%) was calculated as in Figure 4A. The mean values of arrested VemP (%) are shown with S.D. (n ≥ 3 technical replicates) in **B**. (**C, D**) PiXie analysis using the VemP*p*BPA derivatives. Cells used in **A** were analyzed by PiXie as described in Figure 2A. Labeled proteins were subjected to IP with an anti-VemP antibody or pull-down with Ni-NTA agarose and analyzed as in Figure 1. The band intensity of VemP-FL, VemP-APs (described in Figure 2B) in **A** and XLs was quantitated and the mean values (the value at 0.5 min after chase was set to 1) with S.D. (n = 3 technical replicates) are shown in **D**.

# Figure 2-figure supplement 2

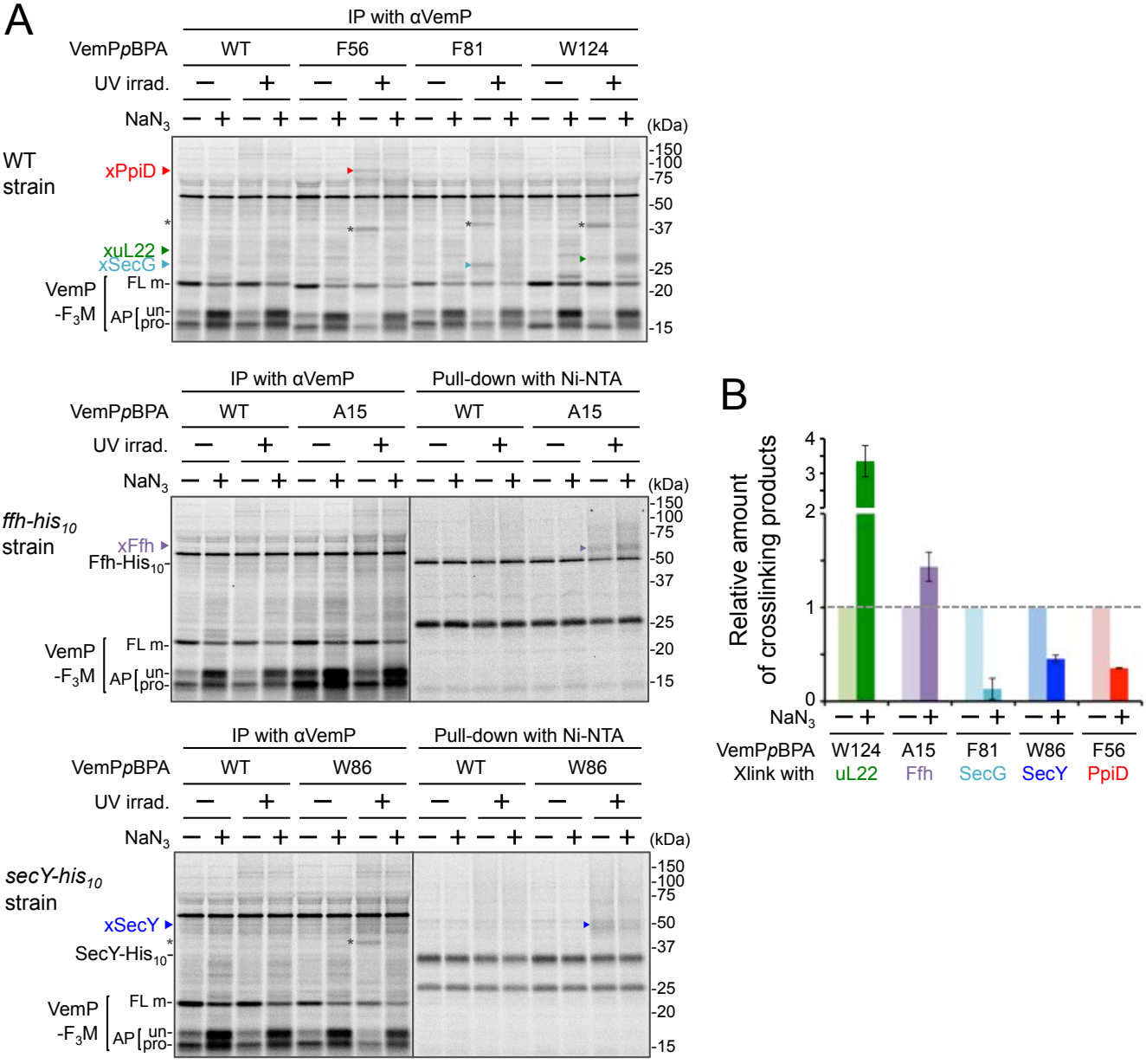


**Figure 2-figure supplement 2 Effect of $NaN_3$ treatment on VemP crosslinking**

(**A**)Wild type cells (***upper gel***) and mutant cells expressing Ffh-$His_{10}$ (***middle gel***), and SecY-$His_{10}$ (***lower gel***) from the chromosome were used. The cells were grown, induced to express a VemP-$F_3$M derivatives with *p*BPA at the indicated position, and analyzed by PiXie as in Figure 1. $NaN_3$ (+) indicates that the cells received 0.02% $NaN_3$ and [$^{35}$S]Met simultaneously. Labeled proteins were subjected to IP with an anti-VemP antibody (**Left**) or pull-down with Ni-NTA agarose (***right***) and analyzed as in Figure 1. Asterisks presumably represent crosslinked dimer forms of full-length VemP-$F_3$M. (**B**) The intensity of these crosslinking bands was quantitated and the relative mean values (the value without $NaN_3$ treatment was set to 1) are plotted with S.D. (n = 3 technical replicates).

# Figure 5-figure supplement 1

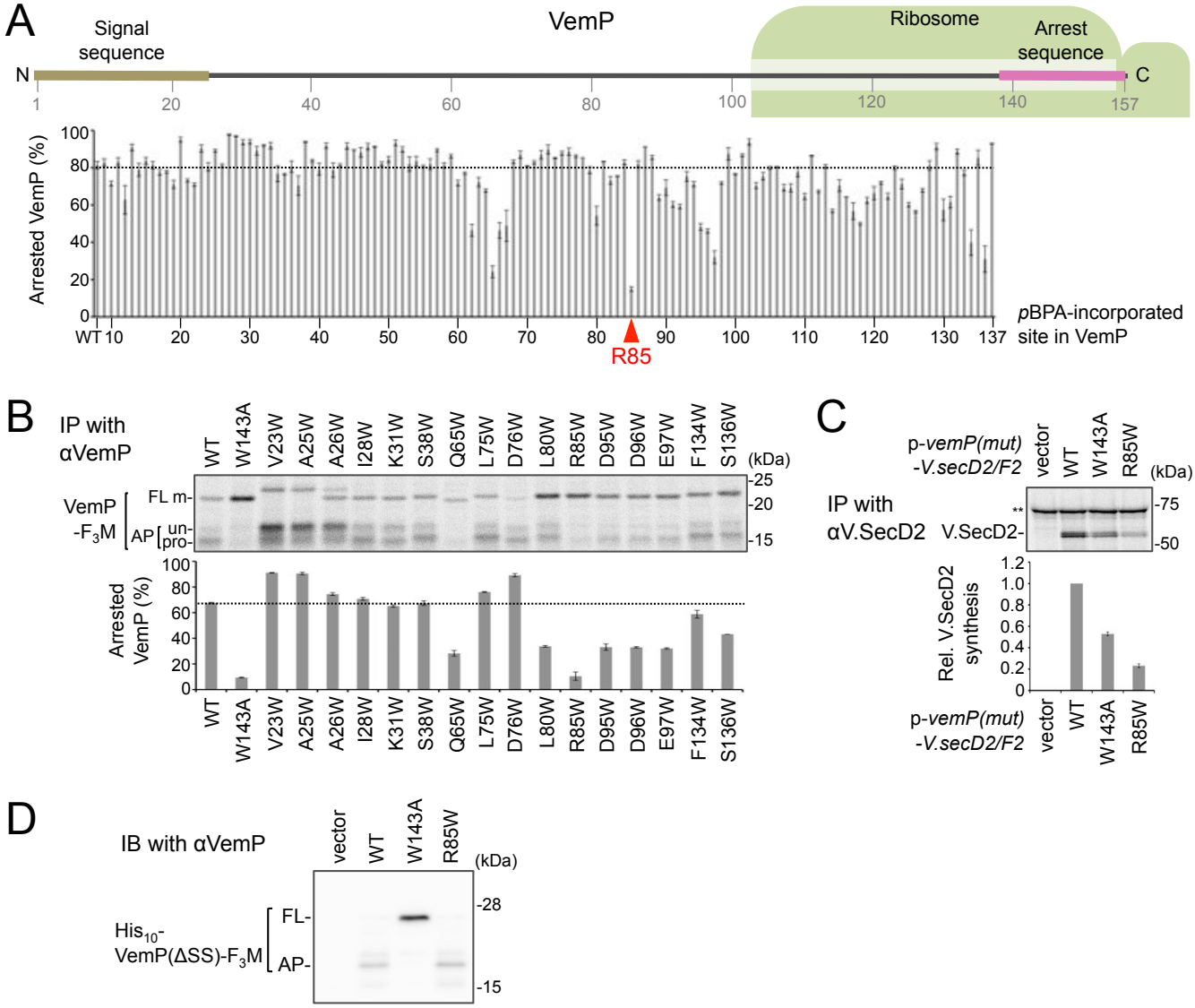


**Figure 5-figure supplement 1 The conserved Arg-85 residue is important for the stability of an arrested VemP *in vivo***

(**A**) Stability of the arrested state of the VemP*p*BPA variants. A schematic picture of the VemP polypeptide in the arrested state is presented with residue numbers. Arrested VemP (%) was calculated from the results in Figure 1. The mean values of arrested VemP (%) are shown with S.D. (n = 2 technical replicates). (**B**) Effects of Trp mutations on the VemP translation arrest. Cells were grown, induced to express the indicated VemP-$F_3M$ derivative, and pulse-labeled as in Figure 1. After 30 sec of chase, total cellular proteins were acid-precipitated, subjected to IP with an anti-VemP antibody and analyzed as in Figure 1. Arrested VemP (%) was calculated and the mean values are shown with S.D. (n = 2 technical replicates). (**C**) WT cells carrying an empty vector or a *vemP-V.secD2/F2* plasmid (the indicated mutation was introduced into the *vemP* gene on the plasmids), were grown and induced as in Figure 1 and pulse-labeled for 1 min. Labeled proteins were then subjected to IP with an anti-V.SecD2 antibody and analyzed as in Figure 1. Double asterisks indicate an un-related protein precipitated with the anti-V.SecD2 antibody. The intensity of V.SecD2 band was quantitated and the relative mean values (the value for WT cells carrying p-*vemP-V.secD2/F2* was set to 1) are shown with S.D. (n = 3 technical replicates). (**D**) Effect of an Arg85 mutation on the translation arrest of a VemP variant lacking its signal sequence. Cells of HM1742 carrying a plasmid, pTV118N-*his$_{10}$-vemP(Δsignal sequence)-3xflag-myc,* into which the indicated mutation had been introduced, were grown, induced with 1 mM IPTG for 60 min, and acid-precipitated. Proteins were analyzed by immunoblotting using the anti-VemP antibody.

# Figure 5-figure supplement 2

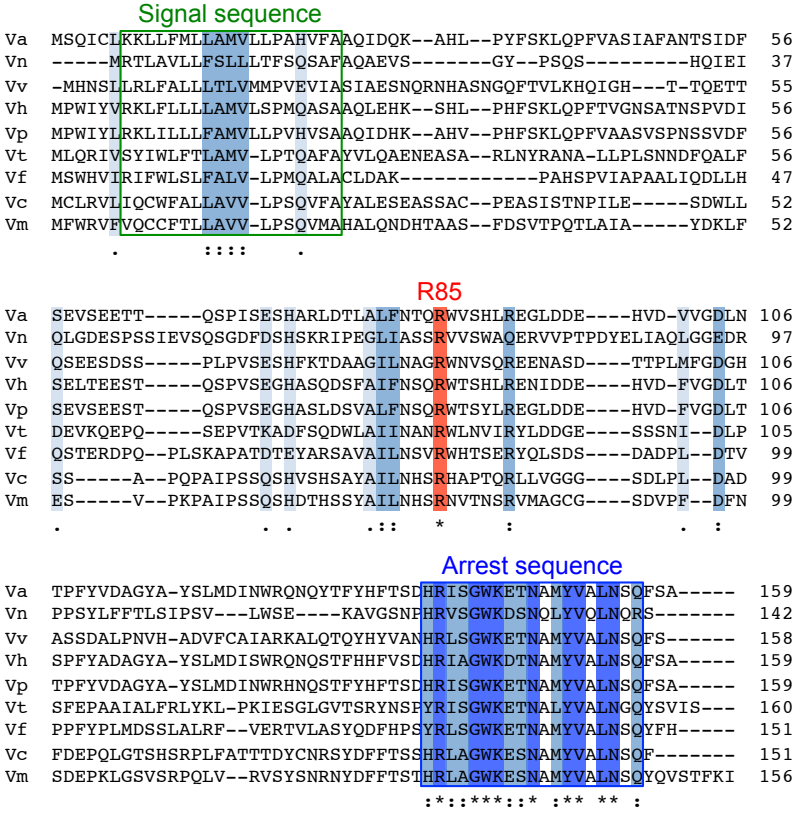


**Figure 5-figure supplement 2 Sequence alignment of VemP orthologues**

Amino acids sequence of VemP orthologues were aligned using Clustal omega program (https://www.ebi.ac.uk/Tools/msa/clustalo/); *Vibrio alginolyticus* (Va), *Vibrio nigripulchritudo* (Vn), *Vibrio vulnificus* (Vv), *Vibrio harveyi* (Vh), *Vibrio parahaemolyticus* (Vp), *Vibrio tubiashii* (Vt), *Vibrio furnissii* (Vf), *Vibrio cholerae* (Vc), *Vibrio mimicus* (Vm). Well-conserved residues, completely conserved residues and the Arg-85 residue are colored in pale blue, blue and red, respectively. The signal sequence and the arrest motif of VemP are boxed with green and blue lines, respectively.